Composite-particle emission in the reaction p+Au at 2.5 GeV

A. Letourneau, A. Bohm, J. Galin, B. Lott, A. Peghaire, M. Enke, C-M. Herbach, D. Hilscher, U. Jahnke, V. Tishchenko, et al.

Composite-particle emission in the reaction p+Au at 2.5 GeV.

A.Letourneau [1] , A.Böhm, J.Galin [2] , B.Lott [3] , A.Péghaire

GANIL, IN2P3/CNRS, DSM/CEA, BP 5027, F-14076 Caen cedex 05, France

M.Enke, C-M.Herbach, D.Hilscher, U.Jahnke, V.Tishchenko

Hahn Meitner Institute, Glienicker Strasse 100 D-14109 Berlin, Germany

D.Filges, F.Goldenbaum, R.D.Neef, K.Nünighoff, N.Paul, G.Sterzenbach

Institut für Kernphysik, Forschungszentrum Jülich GmbH, D-52425 Jülich, Germany

L.Pienkowski

Heavy Ion Laboratory Warsaw University, Pasteura 5a, 02-093 Warszawa, Poland

J.Tõke, U.Schröder

University of Rochester, Rochester, New York 14627, USA

Abstract

The emission of composite-particles is studied in the reaction p+Au at E_p=2.5 GeV, in addition to neutrons and protons. Most particle energy spectra feature an evaporation spectrum superimposed on an exponential high-energy, non-statistical component. Comparisons are first made with the predictions by a two-stage hybrid reaction model, where an intra-nuclear cascade (INC) simulation is followed by a statistical evaporation process.The high-energy proton component is identified as product of the fast pre-equilibrium INC, since it is rather well reproduced by the INCL2.0 intra-nuclear cascade calculations simulating the first reaction stage. The low-energy spectral components are well understood in terms of sequential particle evaporation from the hot nuclear target remnants of the fast INC. Evaporation is modeled using the statistical code GEMINI. Implementation of a simple coalescence model in the INC code can provide a reasonable description of the multiplicities of high-energy composite particles such as $^{2-3}$H and ^{3}He. However, this is done at the expense of ^{1}H which then fails to reproduce the experimental energy spectra.

PACS: 25.40.-h; 25.40.Sc; 24.10.-i; 24.10.Lx; 24.10.Pa

Key words: : Spallation reactions; hot nuclei; excitation energy distribution; production of n, p and composite particles; coalescence model

[1] Present address: DAPNIA/SPhN, CEA/Saclay, 91191 Gif surYvette Cedex, France

[2] Corresponding author:*E-mail address:* galin@ganil.fr (J.Galin)

[3] Present address: CENBG/IN2P3 Domaine du Haut Vigneau 33175 Gradignan Cedex, France

1 INTRODUCTION

The study of spallation reactions induced by protons -either in direct kinematics (protons as projectiles) [1][2][3][4][5][6][7][8][9][10] or in inverse kinematics (hydrogen target)[11][12][13][14], or by ^{3}He[1][2][15], or by antiprotons [6][7][16][17][18][19][20] or by pions[6][7][21], or even kaons[6][7] has been recently given a strong impetus for two main reasons. First, it has been acknowledged that such reactions are quite effective in bringing nuclei to a broad distribution of excitation energies -essentially of thermal origin- without modifying strongly the nucleonic composition of the initial target-nucleus. Thus the heated nuclei are not exposed to the strong collective excitations inherent in collisions between both massive projectile- and target-nuclei. Moreover, since there is only one massive nucleus involved in the reaction, there is only one type of source. In contrast, interpretation of heavy-ion reaction data typically has to contend with several sources of light particles (projectile-like, target-like and intermediate structure). Spallation reactions induced by light projectiles (or in light target-nuclei in the case of inverse kinematics) thus offer a unique test bench for the study of nuclei brought to high temperatures[3]. In particular they allow investigating to which extent the well known, sequential statistical model developed in the early days of nuclear physics works at higher and higher temperatures. Also, for the first time, fission, not induced by a massive projectile and thus not strongly influenced by spin effects and shape distributions, could be investigated in detail either as a function of excitation energy of nuclei initially brought up to temperatures of up to T$\simeq$ 7 MeV[20] or with respect to the isotopic distribution of *all* fission fragments and kinematical properties of the fissioning nuclei[13] .

Thus spallation reactions induced by relativistic light projectiles are subject of interest in their own right, e.g. as far as the mechanism for energy transfer to the target nucleus and the modes of the induced decay of the system are concerned. In addition, these reactions have attracted interest because of their potential applications in the generation of high-intensity beams of neutrons[22][23] (ISIS[24], PSI[25], ESS[26]), muons, neutrinos (e.g. the ISIS facility at Rutherford Laboratories in Europe), or of exotic secondary nuclear species (e.g. ISOLDE-CERN at Geneva, ISAC-TRIUMPH at Vancouver). Spallation reactions have also been considered for the transmutation of nuclear wastes[27][28][29] and/or for developing a new type of nuclear reactor[30][31]. This has triggered systematic investigations of neutron-[6][7][8][10][32][33] and residue-production [11][12][13][14][34][35][36] in thin or thick targets of heavy materials in reactions induced by various hadrons over a broad range of bombarding energies.

All these exciting perspectives for both their fundamental and applied aspects have prompted us to investigate spallation reactions in a very detailed and

original way[1][2][3][4]. For this goal, one needed the experimental information to be as exclusive as possible in order to reach a key quantity in such reactions: the excitation energy brought in by the projectile, on an event-per-event basis. Also, in order to have more constraints for the interpretation of the experimental data, a great effort has been made to consider not only a specific channel but *all* exit channels making up the whole reaction cross section.

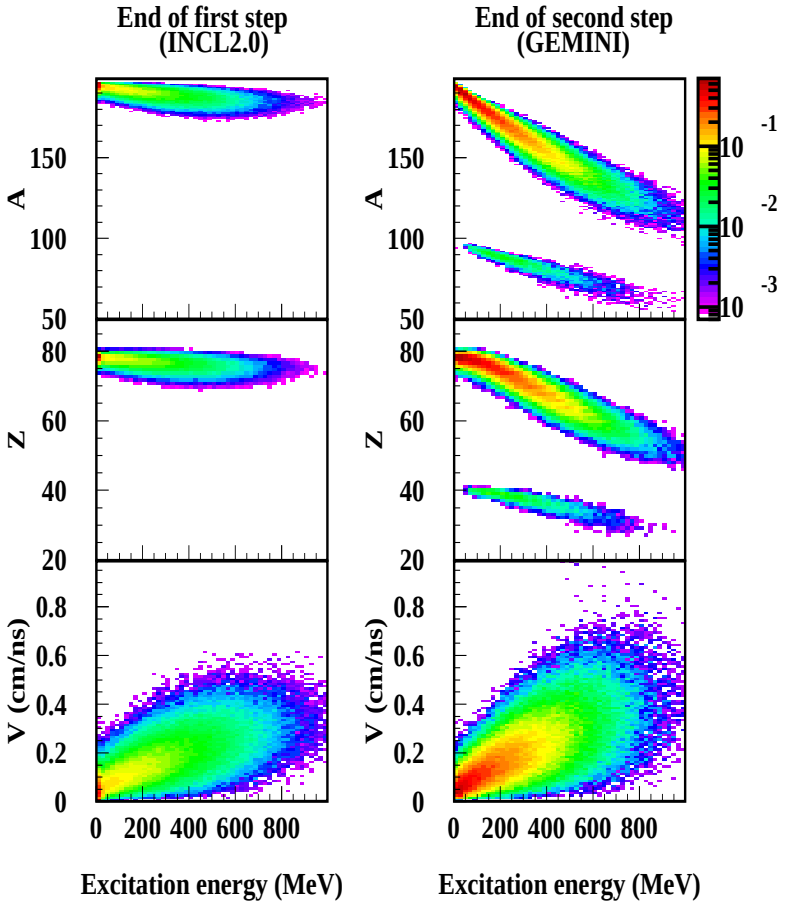

Fig. 1. Monte-Carlo simulation of the 2.5 GeV p +Au reaction using a two-step model, including an Intra Nuclear Cascade step followed by a statistical evaporation/fission stage (for detail see text). The A, Z distributions of the nuclei are given as a function of excitation energy : at the end of the first step (INC) in the left hand panels, at the end of the second step (evaporation/fission) in the right hand panels. The velocity distributions (bottom panel, right) are shown for the evaporation residues, exclusively. Bins in A and Z are unitary, 0.01 cm/ns in velocity and 20 MeV in excitation energy. The z scale (cross sections) is given in mb per corresponding bin squared.

A spallation reaction is currently described as a two-step process. In the first step, the primary nucleon-nucleus interaction is treated as a succession or cascade of nucleonic and mesonic interactions with the nucleons of the target nucleus[37]. In a second step, the resulting excited nucleus is allowed to cool by particle evaporation, as described by equilibrium-statistical models. Figure 1 illustrates predictions made with such a model. Details of the model are discussed further below. The left-hand panels in Fig.1 show the excitation energy (E*) dependence of the A, Z and velocity distributions of the target remnants at the end of the first (INC) reaction step. These results show that the intermediate nucleus remains, within a few A and Z units, similar to the initial Au nucleus (A=197, Z=79) whatever be the excitation energy E*. It is mainly during the cooling stage that many particles can be emitted leaving most residual nuclei (right hand panels) far away in both A and Z from the intermediate nuclei formed (not to consider the fraction of target remnants undergoing fission). The larger the initial excitation brought to the nucleus in the first step of the reaction, the farther the residual nuclei appear to be, with in the extreme cases, a considerable mass loss. These are all the products which are systematically registered in dedicated experiments[5][11][12][13][14]. The small recoil velocities of the evaporation residues shown in the bottom-right panel of Fig.1 illustrate that normal kinematics (proton beam on Au) makes somewhat difficult their direct on-line detection -some products do not exit from the target- and justify the GSI approach consisting in shooting heavy relativistic beams on H targets[11][12][13][14].

If a two-step description of the process can satisfactorily account for the characteristics of the bulk of the light reaction products, as shown in the present study, it remains that composite light particles (^{2}H, ^{3}H, ^{3} He, ^{4}He, ^{6}He, ^{6}Li, ^{7}Li, Be...) exhibit features which cannot be fully described in this simple reaction scheme. Already the early works by Poskanzer et al.[38], Hyde et al.[39] and Westfall et al.[40], as well as the later works by Green et al.[41][42], Ledoux et al.[2] and Fokin et al.[43], demonstrated that the composite-particle emission follows a pattern that differs from statistical evaporation. Obviously at variance with the statistical model are anisotropic emission and the high-energy tails observed in the energy spectra of composite particles. It was also shown that the relative abundance of "equilibrium" composite-particles and "non-equilibrium" ones depends very strongly upon the nature of the considered particle. For instance, neighboring isotopes such as ^{3}He and ^{4}He behave in strongly different ways, with most of emitted ^{4}He being evaporated by the nucleus at thermal equilibrium whereas ^{3}He, on the contrary, is mostly emitted prior to thermal equilibration.

The mechanisms responsible for composite-particle emission before equilibration are not well understood. Different possibilities have been proposed in order to explain the origin of composite-particles with momenta close to that of the incident projectile. The hypothesis that the preformed particles at the

surface of the nucleus can be emitted in a direct knock out reaction is certainly not the unique explanation as shown in the study of 800 MeV p on different target nuclei[44]. Indeed, light target-nuclei, like ^{12}C, which are mostly surface-nuclei and have, in addition, a large alpha-particle component in their ground state wave function do not favor alpha-particle emission as would be expected in such a model. In contrast, the so-called "snowball" mechanism which consists of a succession of pick-up reactions looks more appropriate in order to understand the forward production of ^{3}He and ^{4}He in 800 MeV proton induced reactions on different target nuclei[44]. In such a scheme the proton picks up a neutron (or a proton) to form a deuteron through the reaction $p + n \longrightarrow d + \pi^0$ (or $p + p \longrightarrow d + \pi^+$). In one additional pick up, ^{3}He is reached through $d + p \longrightarrow^3 He + \pi^0$ or in $d + n \longrightarrow^3 He + \pi^-$and then ^{4}He through either $^3He + n \longrightarrow^4 He + \pi^0$ or $^3He + p \longrightarrow^4 He + \pi^+$.

Besides the direct processes giving rise to forward directed emission of composite-particles[45], an indirect process has been considered as contributing at any angle by coalescence of two nucleons (or by coalescence of a nucleon with an already preformed composite-particle obtained through the same coalescence mechanism) with the involved particles close enough in phase space. When the pair possesses a wave function that strongly overlaps with the composite-particle wave function, the particles may fuse due to final state interaction. This non-direct mechanism for composite-particle production was first discussed by Butler and Pearson[46]. A coalescence model was successful in interpreting the deuteron production in proton induced reactions between 150 MeV and 500 MeV bombarding energy[43]. However, it is not clear whether such a phenomenological approach can explain the build-up of composite-particles more massive than deuterons in either one-step or multi-step processes.

In this paper, we investigate in detail the conditions under which the composite-particles ^{2}H, ^{3}H, ^{3}He, and ^{4}He, are emitted in the 2.5-GeV p+Au reaction. This has been made possible due to the coincident detection of neutrons and charged particles, both over 4π and with high detection efficiency. From these multiplicity data one is able to infer the excitation energy, E*, event-wise. One particular issue investigated in the present work is how the emission of non-equilibrium composite-particles depends on E* or less directly on the impact parameter.

The paper is organized as follows: in the next section, the experimental set-up and the data analysis are described. In Section 3, data related to excitation energy determination are reviewed. In section 4, a detailed analysis of non-evaporative, composite-particle emission patterns is discussed. Section 5 contains a summary of the conclusions.

2 EXPERIMENTAL ASPECTS AND DATA ANALYSIS

2.1 EXPERIMENTAL SET-UP

The experiment was performed at the COSY accelerator in Jülich with a 2.5 GeV proton beam impinging on a 8.62 mg/cm^2 thick Au target, inclined at an angle of 45° with respect to the beam axis.

The thickness of the self supporting target was determined by areal weight and further checked by energy loss measurements of α-particles from ^{212}Bi and ^{212}Po. The 25 x 27 mm^2 target was glued on a 0.2 mm thick Al frame with a central opening of 20 mm in diameter. An identical empty frame, mounted on the same pole as the target frame, was used for background measurements, before and after the target irradiation. The background was always observed as negligible in the yields of the telescopes (to be described later). The target was mounted at the center of two concentric 4π detectors, the Berlin silicon ball (BSiB) for detection of charged particles[47] and the Berlin scintillator tank (BNB) for neutron detection[7].

The BSiB consists of 162 (148, in the present experiment) silicon detectors (500 μm thick) making up a sphere with a diameter of 20 cm. A detailed description of the BSiB can be found in Enke et al [3] [4]. For each BSiB detector, three signals were collected: the time-integrated charge and amplitude of the signal, allowing pulse shape discrimination and Z identification and the time of flight permitting mass determination. The start signal was provided by an in-beam plastic scintillator mounted 11.2 m upstream of the target while the stop signal was derived from the Si detectors. The total time resolution is about 0.9 ns. The energy calibration of the Si detectors was made with α-particles of ^{241}Am, ^{212}Bi and ^{212}Po sources. The detectors acted either as stop detectors or ΔE detectors, depending on the nature and energy of the considered particle. Details about particle identification can be found in Lott et al.[18].

Due to the single layer of 500 μm thick Si detectors, the accessible energy range of charged particles was limited up and down. The lower energy cutoff was intrinsically low (2.2 MeV$\pm$ 0.3 MeV) and similar for all kinds of light particles. The upper cutoff was determined for those particles punching through with an energy deposition equal to the lower threshold. It amounts to 26$\pm$4, 49$\pm$6 and 76$\pm$7 MeV for ^{1}H, ^{2}H and ^{3}H, respectively. The produced He isotopes and heavier particles were not affected by the upper threshold. The most energetic

[4] Recent precise calibrations of the BSiB geometrical efficiency[48] have shown that the global efficiency of 80% given in ref.[3] has to be decreased by (8$\pm$2)%. We have checked that such a reduction of the efficiency has only minor consequences on what is developed in the present paper.

H isotopes and all pions arising from the first step of the reaction were not observed. The problems of limited energy range for H detection as well as of modest isotopic resolution were solved at 30 °, 75 ° (twice), 105° (twice) and 150° by replacing the 500 μm detectors by telescopes. The latter were made of successive 80 μm, 1000 μm ΔE-Si detectors backed by a 7 cm thick CsI detector with a photo-diode readout and sustended solid angles of about 2.10^{-3} of 4π sr, each. The lower energy cuts were somewhat higher for the telescopes due to the requirement of the particle punching through the 80 μm thick detector. These thresholds amounted to 2.8 MeV for ^{1}H, 3.6 MeV for ^{2}H, 4.1 MeV for ^{3}H, 15 MeV for ^{3}He and ^{4}He and 26 MeV for Li isotopes. As will be shown later on in Fig.3 and Fig.4, these values are well below the Coulomb energies for emitters having masses close to 200. The energy calibration of the Si detectors was also performed with the Am source while the CsI response was calibrated on-line by means of well identified particles traversing the Si detectors. The mass resolution was excellent up to Be, B isotopes detected by the 80μm-1000μm pair of Si detectors.

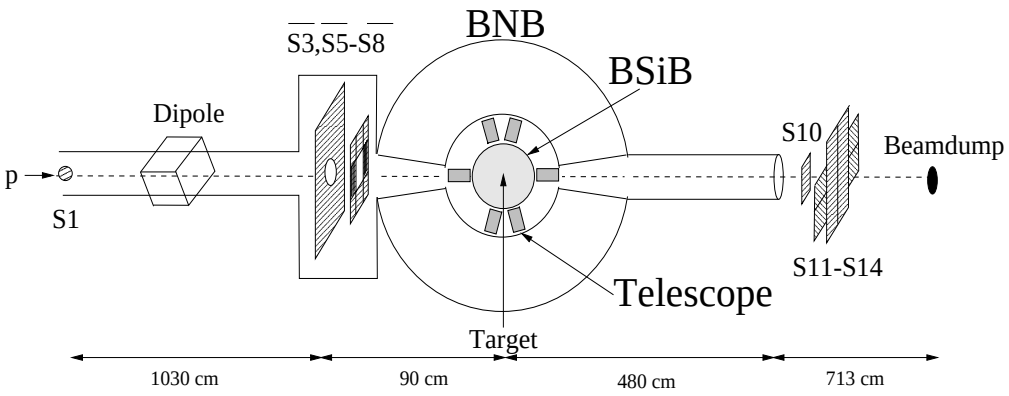

Fig. 2. Layout of the experimental set-up (not to scale), with the central Berlin Neutron Ball (BNB), the Berlin Si Ball (BSiB), the 6 telescopes and the auxiliary plastic scintillator detectors (for detail see text), including the in-beam start detector S1. The position of the different elements is given by the bottom scale.

The BNB is a spherical shell containing 1.5 m^3 liquid scintillator with an inner and outer diameter of 40 cm and 140 cm, respectively. The scintillator was loaded with Gd (about 0.4 % in weight). The signal induced in the BNB by a nuclear reaction is made of two distinct components separated in time[49]. The prompt component induced by γ rays, energetic charged particles (those crossing the inner wall of the BNB) and neutrons was used to infer a nuclear reaction and was also utilized as a timing signal. A delayed signal occurred each time a neutron, once thermalized, was captured by a Gd nucleus. Counting these signals over a period of 44 μs after a reaction event has been detected provided the neutron multiplicity. The detection efficiency for evaporated neutrons (with a few MeV kinetic energy) was about 85% as checked continuously during the experiment, using a ^{252}Cf neutron

source as a reference. For more energetic neutrons, arising during the first steps of the p-nucleus collision, the efficiency dropped down rapidly (about 40% and 15% for 30 and 100 MeV, respectively). The actual overall detection efficiency can be computed using a Monte-Carlo simulation model assuming a given neutron energy distribution[3]. The overall neutron detection efficiency increased from about 50% for the most peripheral collisions (those generating the largest fraction of non evaporative neutrons) to nearly 80% for the most dissipative collisions (when nearly all emitted neutrons are evaporated). As will be shown later on, the neutrons of interest for inferring the excitation energy event-wise were the evaporated neutrons which were always measured very efficiently whereas the high energy neutrons (then considered as parasitic in the counting) were weakly detected but nevertheless taken into account.

The trigger for the presented data was provided either by the fired Si detector(s) of the BSiB or by the second member (1000 μm thick Si detector) of one of the telescopes.

The whole experimental set-up is sketched in Fig.2 with the two balls, BNB and BSiB -as the main and central part of the equipment- and auxiliary plastic beam detectors labeled S_1, S_3, S_5-S_8, S_{10}, S_{11}-S_{14}. The S_1detector, 0.3 mm thick and 20 mm in diameter, positioned 11.2 m upstream from the target was the start detector counting up to about 10^6 pps. The S_3 and S_5-S_8 detectors, located at about 1 m upstream of the target, were veto detectors, used in order to tag all off-axis protons. The focus of the main beam at the center of the target was about 2 mm in diameter on a quartz in target position. The S_{10} detector was used to cross-check the S_1 counting and S_{11}-S_{14} were utilized for focusing and aligning the beam on axis. The beam normalization for determining cross sections was obtained from the counting of S_1 corrected for off axis protons detected by either S_3 or S_5-S_8. A dead time correction for data acquisition was made.

2.2 EXPERIMENTAL DATA AND THE EVENT-WISE EXCITATION ENERGY DETERMINATION

The energy spectra are given for all particles detected at 30° , 75°, 105° and 150° in Fig.3 and Fig.4. As already was shown earlier by Poskanzer et al.[38], all particles exhibit a rather similar evolution of their energy spectrum with angle, with an "evaporation-like", low energy component at all angles and a high energy tail, more pronounced in the forward direction. The intensity of the first component does not depend sensitively on the emission angle in contrast with the high-energy component decreasing in intensity with increasing emission angle. The solid lines (dotted line for ^{1}H) in Fig.3 and Fig.4 represent the evaporation component as it is obtained in a full simulation to be described

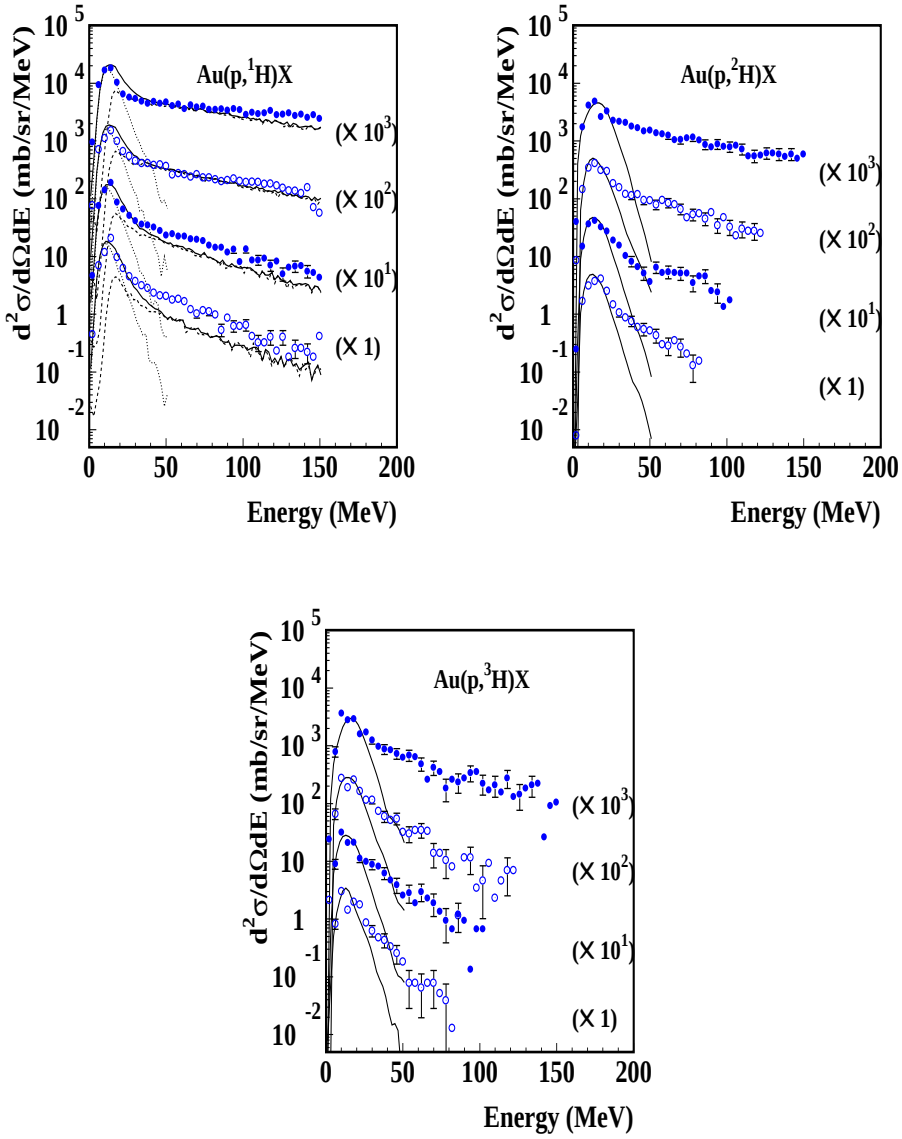

Fig. 3. Doubly differential cross sections for the production of the H isotopes as measured by the telescopes set at 30°, 75 °, 105° and 150°, from top to bottom in each panel (dots). For ^{1}H, the dotted, dashed and solid lines result from the second stage (evaporation), the first stage (INC) and their sum, respectively, of a two-step Monte-Carlo simulation (see text). For ^{2}H and ^{3}H the evaporative contributions are shown by solid lines.

later on in this paper. It is worth noting that about 1/3 of the α-particle production proceeds through the primary evaporation of the unstable nucleus ^{5}He which is implemented in the GEMINI code[4]. It should be stressed that, due to the large straggling in the recoil velocity of the emitters -as shown in Fig.1- the measured spectra cannot be transformed *globally* in the c.m. system

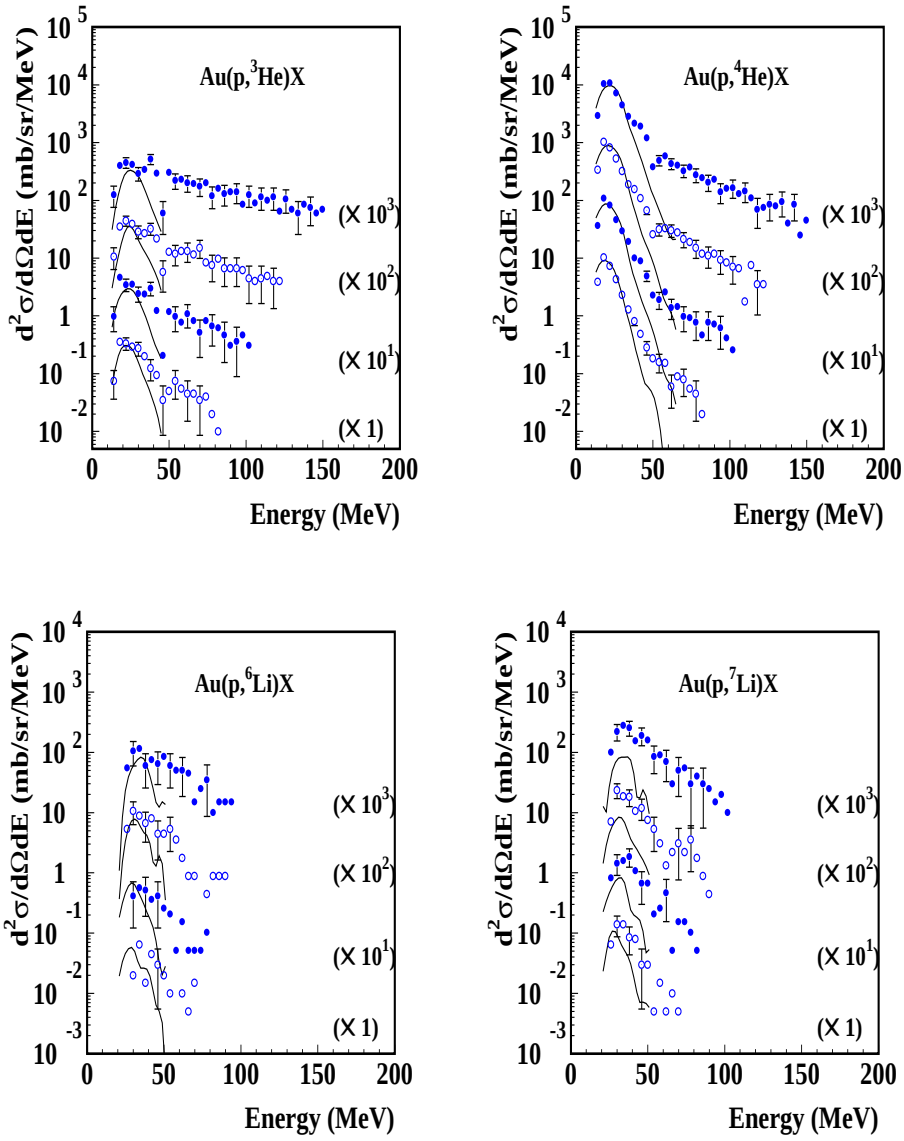

Fig. 4. same as Fig.3 (^{2}H and ^{3}H) for He and Li isotopes.

to be compared with the model data but the comparison can only be made the other way around, with the modeled data transformed event-per-event in the lab system, as done here. The ratio between the low-energy evaporative component and the high-energy component depends strongly upon the nature of the considered isotope. This is best seen for ^{3}He and ^{4}He with the high energy component rather strong for ^{3}He when compared to the low energy one and weak for ^{4}He. Such an observation had already been made at 300 MeV[41][42] and 5.5 GeV[38] bombarding energies and thus appears to be a quite general feature in a broad energy range for proton induced reactions. This distinct behavior for ^{3}He and ^{4}He reaction products has also been noticed

in heavy-ion induced reactions[50] and attributed to different emission times. The experimental energy-integrated cross sections, given in Table 1, are all shown in the left panel of Fig.5 as a function of emission angle and are then compared to the simulated evaporative part (right hand part with thick lines). ^{3}He is much more forward peaked than ^{4}He and this is clearly due to the quite different strength of the non-evaporative part for the two isotopes.

Particle	30^o	75^o	105^o	150^o
^{1}H	818± 62	560±42	465±35	394±30
^{2}H	219±19	141±12	118±10	98±8
^{3}H	106±9	70±6	65±5	52±4
^{3}He	28±3	18±2	14±1	9.1±0.8
^{4}He	200±17	156±13	146±12	128±11
^{6}He	3.2±0.4	2.3±0.3	2.1±0.2	1.8±0.2
^{6}Li	3.6±0.4	2.6±0.3	1.3±0.1	1.0±0.1
^{7}Li	7.7±0.8	4.9±0.5	3.9±0.4	2.4±0.3

Table 1
Energy integrated cross sections (mb/sr) at four detection angles for all measured lcp. The given errors include statistical and systematical errors. The integration ranges on energy are 2.8-200 MeV , 3.6-200 MeV, 4.1-200 MeV for ^{1}H, ^{2}H, ^{3}H, respectively and 15-200 MeV and 26-200 MeV for H, He and Li isotopes, respectively.

The detailed account of the angle-integrated cross sections as they are measured and as they can be split between evaporative particles -obtained by the model simulation- and non-evaporative particles -obtained by the difference- is provided in Table 2, together with the fraction of non-evaporative particles. As shown in Fig.6, the latter fraction depends strongly on the nature of the considered particle and results from a complex interplay between the different properties of the latter: mass, atomic number, binding energy, nuclear density. Also, as already noticed in previous investigations[2][39][41], even more massive composite-particles like Li isotopes clearly exhibit a non-equilibrium component (Fig.4).

The data of the present experiment have been compared with the prediction of a two-step model including an Intra Nuclear Cascade (INC) followed by a statistical deexcitation when the nucleus achieves thermal equilibrium. As shown in a previous article[3], the often used INC approach first developed by Bertini[51] and later included in High Energy Transport Codes (HETC) such as LAHET[52] or HERMES[53] fails to reproduce spallation data on heavy targets by strongly overestimating the amount of energy deposited by the incident proton in the target nucleus. A much better agreement has been recently

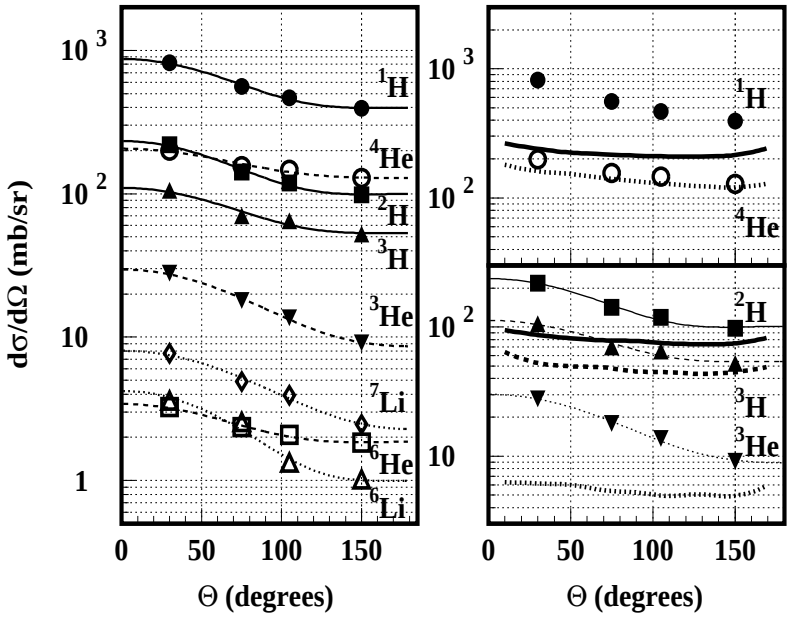

Fig. 5. Left: angular distributions of the reaction products given in (mb/sr) as measured (symbols) and as fitted with Legendre polynomials (lines). The integration ranges on energy are 2.8-200 MeV , 3.6-200 MeV, 4.1-200 MeV for ^{1}H, ^{2}H, ^{3}H, respectively and 15-200 MeV and 26-200 MeV for He and Li isotopes, respectively. Right: the experimental data (symbols and thin lines for ^{2}H, ^{3}H,^{3}He) are compared with the simulated evaporative component from the two-step model (thick lines).

reached[3] with the improved INCL2.0 version of the INC code developed by Cugnon[54][55]. This code has been utilized to investigate the 2.5 GeV p+Au reaction, with the second step of the reaction being treated with the evaporation/fission code GEMINI[58]. Standard parameters have been used and no attempt has been made to optimize the parameters. In the INCL2.0 code, the depth of the potential well was set to V_0=-40 MeV and the inelastic reaction cross section was normalized to σ_{inel}=1743 mb[3]. In the GEMINI code (version 5/97), the level density parameter was set to a=A/10 MeV^{-1}, a_f/a_n=1.0 and symmetric fission was assumed. The incoming wave boundary condition (IWBC option) for calculations of the transmission coefficient was used.

As shown in Fig.3, the simulation for ^{1}H production considers the two steps of the process (given by the dotted and dashed lines for evaporation and INC emission, respectively, and by the solid line for their sum) whereas for composite-particles (Fig.3 and 4), only the second step (evaporation) is considered (solid line). The overall agreement at low energy (close to the emission barrier) is rather satisfactory for all considered particles (except ^{7}Li) at all emission angles indicating that evaporation is correctly accounted for. This is best shown at 150°, where evaporation is the dominant component for all particles. This good agreement means that the excitation energy distribution at the end of INC is properly described by the employed INC model, as was also already noticed[3] at 1.2 and 1.8 GeV bombarding energies. Also, the high energy part of the ^{1}H spectra is rather satisfactorily reproduced at most angles by the INC model. This good agreement gives already some confidence in the employed model. As will be shown further below, the multiplicity distribution data for both charged particles and neutrons give additional support to the reliability of the simulation.

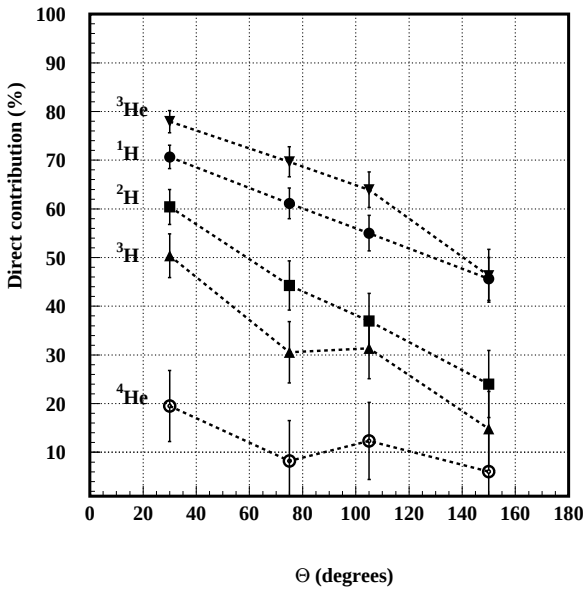

Fig. 6. Fraction of the deduced direct (i.e. non evaporative) emission to the totally measured production for H and He isotopes, as a function of emission angle.

The measured correlated distribution between neutron and light charged particle multiplicities (coloured contours) is shown in Fig.7 (lower right panel) together with the simulated one after correction for detection efficiency (contour lines). The simulated data using the INCL2.0 and GEMINI codes are first shown as obtained without any correction of detection efficiency, summed over the two steps of the reaction (upper left panel) or during the evaporation stage

only (upper right panel). For completeness, we note that the simulation includes the production of spurious neutrons from secondary reactions induced by high energy cascade particles (E>150 MeV) with either the BNB shell (2-3 mm of stainless steel) or the scintillator liquid. On the average, from the neutrons thus produced, only about one is detected.

	σ_{total} (b)	$\sigma_{evaporated}$ (b)	$\sigma_{total} - \sigma_{evaporated}$ (b)	$\sigma_{direct}/\sigma_{total}$
^{1}H	6.98±1.04	2.75±0.06	4.23±1.10	60%
^{2}H	1.77±0.29	0.99±0.03	0.78±0.32	45%
^{3}H	0.90±0.13	0.59±0.02	0.31±0.15	35%
^{3}He	0.21±0.04	0.068±0.009	0.14±0.05	70%
^{4}He	1.96±0.30	1.74±0.04	0.22±0.34	10%
^{6}He	0.027±0.005	not implemented		
^{6}Li	0.025±0.006	0.022 ± 0.005	0.003 ±0.011	
^{7}Li	0.056 ± 0.012	0.026 ± 0.006	0.03 ± 0.018	

Table 2
Energy- and angle-integrated production cross sections: as determined from the telescopes (first column), as simulated for evaporative particles (second column), as deduced by difference for non-evaporative particles (third column). The last column provides the fraction of non evaporative particles. For energy limits and error bars, see table 1.

It is clearly shown that at 2.5 GeV bombarding energy the evaporation stage provides most of the emitted particles (comparison between the upper panels in Fig.7). From a comparison between the upper left and lower left panels, it can be concluded that the consideration of the energy-dependent detection efficiency only weakly affects the pattern of the whole picture, just shrinking it. The remarkable agreement between the measured data and fully simulated ones (lower right panel of Fig.7) is also highlighted in some more detail in the projections of these multiplicity distributions presented in Fig.8 for neutrons, Z=1, Z=2 particles and their sum (denoted by lp: light particles). The experimental data are presented by dots, the efficiency uncorrected simulated data by dashed histograms and the efficiency corrected ones by solid histograms. The shaded areas result from the additional condition that at least one charged particle is detected. As a consequence, for meaningful comparisons between experimental data (solid dots) and simulated ones, the shaded areas must be considered.

One may wonder why good agreement between simulated data and experimental data (Fig.8) is obtained, even though composite particles are also emitted in non-evaporative processes which are neglected in the calculations. The rea-

son is that the non-evaporative composite-particle contribute about 24% in the charged particle balance but only 12% once filtered by the high energy detection thresholds of the 4π detector array.

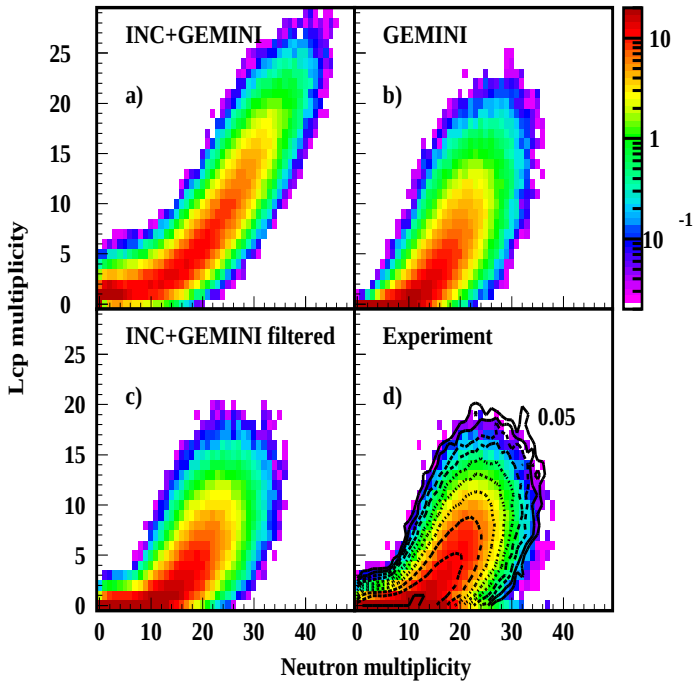

Fig. 7. Production cross sections (z coloured scale, expressed in mb per M_n and M_{lcp} units) as a function of lcp and neutron multiplicities. a): as directly obtained from the *two* steps of the Monte-Carlo simulation (see text). b): as obtained from the second step only (evaporation). c): the data from a) have been filtered by the detector acceptances (or energy dependent efficiency for the neutrons) d): the shaded plot represents the measured data and the contour lines, the simulated data shown in c), thus allowing direct comparison. Successive contour lines represent a doubling in cross section with the lower level at 0.05 mb per unit neutron and lcp multiplicities.

With the model calculations providing good agreement with the bulk of the experimental data, one can make use of this model in order to infer the excitation energy. The latter is given in Fig.9 at the end of the INC step and was deduced by a procedure to be described in the following. As was shown in a previous article[1], the intra-nuclear cascades are followed by the time-dependent INC program until the deposited energy was found to be statistically distributed over all nucleons in the target remnant, such that subsequently emitted particles showed thermal emission patterns, i.e., isotropic angular distributions and Maxwell-Boltzmann energy distributions. In the INCL2.0 version of the

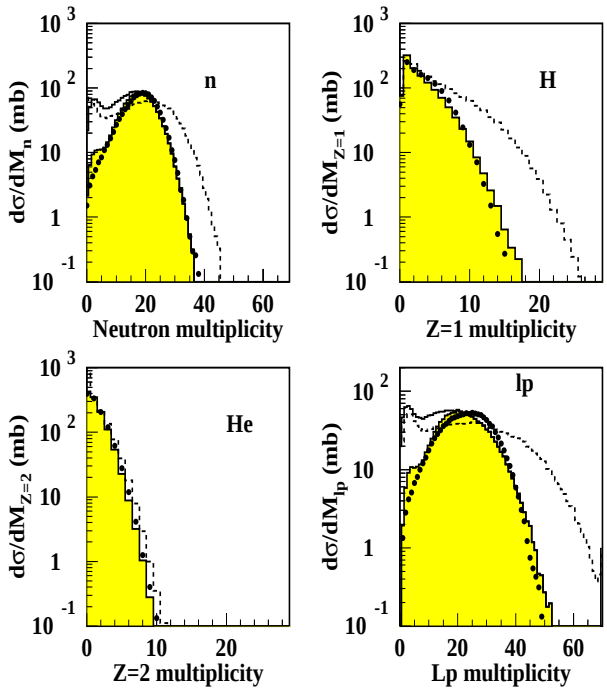

Fig. 8. Multiplicity distributions of the neutrons (n), summed hydrogen isotopes (H), summed He isotopes (He) and their sum (Light particles: lp). Dots: as measured with the trigger condition (Mlcp$\geq$1). Dotted histograms: as Monte Carlo simulated (see text). Solid histograms: as Monte Carlo simulated and corrected by detector acceptances (energy dependent efficiency for the neutrons). Shaded areas: as before with the additional condition (Mlcp$\geq$1) to allow direct comparison with experimental data (dots).

INC Liège code, there is an option (called thereafter "default option") allowing the thermalization time to be automatically determined as a function of the impact parameter. The presented data are actually obtained by using this "default option". It is checked on α -particles, the only particles which are more than 85% evaporation-like particles, that the multiplicity of these particles is reproduced when using the default option. It can be shown, by changing arbitrarily the equilibration time to values of 20 fm/c and 30 fm/c for all impact parameters, that this time greatly influences the amount of evaporated α-particles (Fig.10) and the excitation energy distribution (Fig.9) and that the best agreement is found with the "default" option. The *average* default time is found to be $<t_{eq}>$=22.7 fm/c. Verifying that the chosen cutoff time for the INC calculation is properly matched to the energy equilibration time, e.g., by the above test involving α-particles, is crucial for a reliable determination

of the excitation energy, E*.

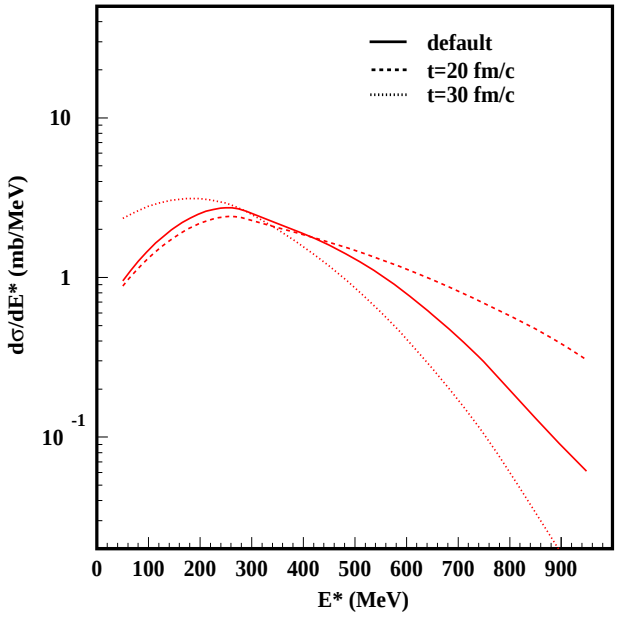

Fig. 9. Excitation energy distributions under the condition that $M_{lcp}>1$ and as directly given at the end of the INC stage of the Monte-Carlo simulation with several equilibration times. The impact parameter dependent "default" time is found to be 22.7 fm/c on the average. Note that in contrast to the "default" option which is impact parameter dependent, the 20 and 30 fm/c simulations have been run without such a dependence.

In our previous work[3][16][18], we have established a method to deduce the excitation energy remaining in the nucleus after the fast INC interaction from a comparison of the total number of detected light particles with the one calculated from an evaporation code, e.g. the code GEMINI. In the present analysis some refinements have been introduced to this method: we simulate the entire reaction and use the predicted multiplicities of neutron and charged particles from the two reaction stages, including appropriate corrections for spurious particles and detection losses, to "calibrate" the experimental (M_n, M_{lcp}) data in terms of the average excitation energy $E^*=E^*(M_n, M_{lcp})$. Also, E^* is determined no longer from the simple summed number of indistinguished neutral and light charged particles but rather from their two separate numbers. This distinction has also been shown very useful in interpreting data from heavy-ion collisions[56][57].

Fig. 11 displays a two-dimensional contour diagram of $<E^*>$ vs. M_n and M_{lcp}

predicted as explained before. All appropriate corrections have been applied to the simulated data. In the following discussion, to every measured event, a corresponding average excitation energy E* has been estimated based on the coincident multiplicities (M_n, M_{lcp}) and in accordance with the calibration function E*(M_n, M_{lcp})

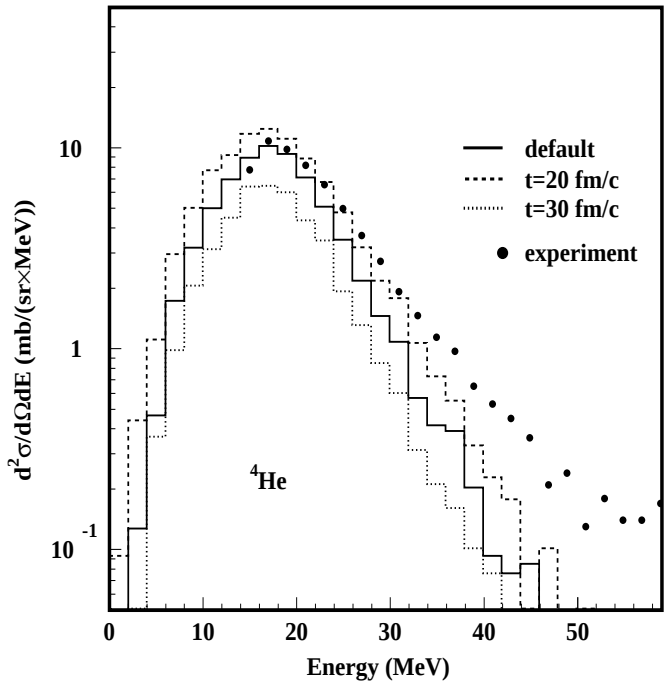

Fig. 10. Energy distribution of ^{4}He, as measured with the telescope at 150° (dots) and as given by the INCL2.0 + GEMINI Monte-Carlo simulations (histograms) with different switching times for the INC process including the one given by default by the code. For detail see text.

Fig. 12 illustrates estimates for the systematic uncertainties associated with the determination of the average excitation energy <E*> from measured particle multiplicities (M_n, M_{lcp}). The top panel provides absolute "error bars" corresponding to ± one sigma value while the bottom panel shows the relative uncertainties σ_{E*}/E* in the determination of E*. Reasons for an inferior resolution at lower excitations include a relatively lower number of particles and more significant effects of efficiency corrections for particles being dominantly of non-evaporative character.

At very large E*, the absolute uncertainty is also greatly influenced by efficiency effects which become crucial in the tail of a distribution. It should be

noted that without detecting the neutrons -as in most experiments- the accuracy of the E* reconstruction would be further reduced. Indeed for a given lcp multiplicity, the neutron multiplicity distribution is very broad. Assuming event-per-event a single *average* neutron multiplicity, as often done in attempting to correct for neutron evaporation without measuring the neutrons, deteriorates further the E* reconstruction.

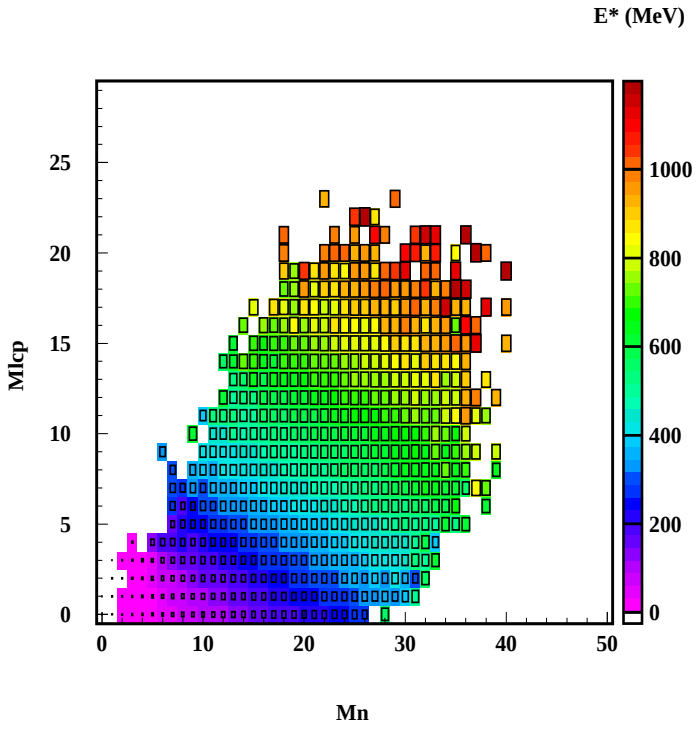

Fig. 11. The matrix provides E* (coloured code running on the right hand side as well as the size of the box proportional to E*) as a function of neutron and lcp multiplicities, as obtained from the simulation and considering both INC- and evaporated particles. The acceptance and detection efficiency corrections are made on the given multiplicity values such that the matrix is directly usable as an abacus for determining E* on an event-per-event basis from the measured multiplicity data.

One may wonder why a distinction between Z=1 and Z=2 particles has not been made in our approach to infer E*. As a matter of fact, both types of evaporated particles remove a similar amount of energy when emitted, simply because for heavy emitters their difference in binding energy is roughly counterbalanced by the difference in Coulomb energy.

As a last remark, the reconstructed E* distributions using the method described by Enke et al.[3] or including the refinements of the present approach do not exhibit sensitive differences. This stems mainly from the fact that the iso E* contours of Fig.11 are rather parallel in the Mlcp-Mn plane once all

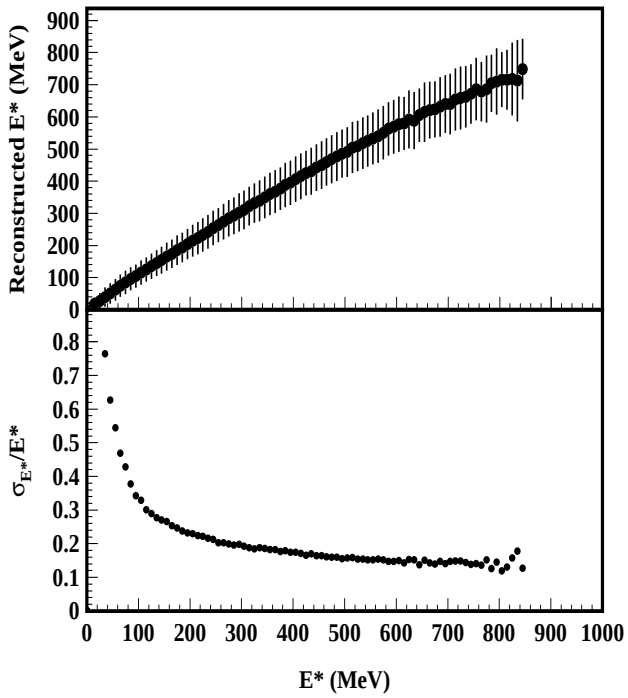

Fig. 12. The upper figure expresses for each E* bin as given by the Monte Carlo simulation (i.e. at the end of the INC step) the reconstructed $< E^* >$ from Fig.11, using the simulated multiplicities of n and lcp. The error bars correspond to $\pm$ one sigma deviation. The relative uncertainty (σ_{E*}/E*) in the determination of E* is shown on the bottom figure as a function of E*.

emission and detection effects are taken into account, thus showing that the distinction between neutrons and lcp has only a weak effect on E* determination.

3 COMPOSITE-PARTICLE EMISSION

As already shown before in Fig.6 and Table 2, a sizeable fraction of the detected composite-particles is not emitted during the evaporation stage and cannot be accounted for with the two-step model used so far. This is also shown in Fig.13 and in Table 3 in terms of average particle multiplicity as a function of excitation energy, the latter estimated from the measured multiplicities (M_n, M_{lcp}) as explained above. The experimental data represented by symbols in Fig.13 include all charged particles detected by the telescopes,

integrated over detection angle and kinetic energy. These data are compared with theoretical multiplicities (curves in Fig. 13) obtained from calculations based on evaporation only. Again, corrections for detection efficiency have been applied to the results of the calculations. The difference between the two sets of data evolves with excitation energy in a rather systematic way: The lower the excitation energy, the larger the contribution of non-evaporative particles appears to be. At the highest excitation energies, i.e., for the most complex INC's, emitted particles are mostly due to statistical evaporation. It is also observed, qualitatively at least, that non-evaporative proton and composite particle patterns develop with excitation energy in very similar fashion. This hints to a common origin of these components. For example, the composite-particles could be formed in the occasional coalescence of several non-statistical nucleons.

It is instructive to examine the evolution of the proton energy spectra with emission angle and with increasing excitation of the target remnant. In Fig.14, a comparison is made between experimental data (dots) and the total theoretical spectra (solid line) including evaporation and non-statistical particles, when coalescence is ignored in the simulation calculations. Even though qualitative agreement is obtained between data and simulations, the simulations often over-estimate the low energy component and miss the slope of the high-energy component.

An enlargement of the low energy part of the spectra measured at 30° and at 150° and a decomposition of the simulated spectra into their different components (Fig.15) reveals several interesting features. One can distinguish three energy zones: up to about 15 MeV, evaporation (shaded areas) is dominant, above 40 MeV, direct emission (dashed curves) is dominant and, in between, the two processes contribute more evenly but with different weights at 30° and 150°. For all excitation energies and emission angles, the simulations reproduce relatively well the evaporation part (E<15 MeV) of the spectra. Particle energy spectra in the range15 MeV<E< 40 MeV are still well described at backward angles (150°), where evaporation is dominant. At more forward angles (30°) where the more directly emitted particles dominate, the agreement is less satisfactory. In the latter case, the sum of the direct and evaporative components as they are simulated (solid histograms) over-estimates the experimental data for all excitation energy bins. At higher energies (Fig.14 and Fig.15) (for E>100 MeV at 30° and for E>40 MeV at 150°), the model calculations under-estimate the experimental data for all considered excitation energy bins. How can all these features be interpreted? In so far as the evaporative character of the ejectiles is considered, the good agreement given by the model for the protons reinforces what has been already stressed before for ^{4}He: The INC step of the hybrid model accounts very well for the total excitation energy deposited in the target remnant, while the statistical evaporation model (GEMINI) provides a realistic picture of the distribution of this

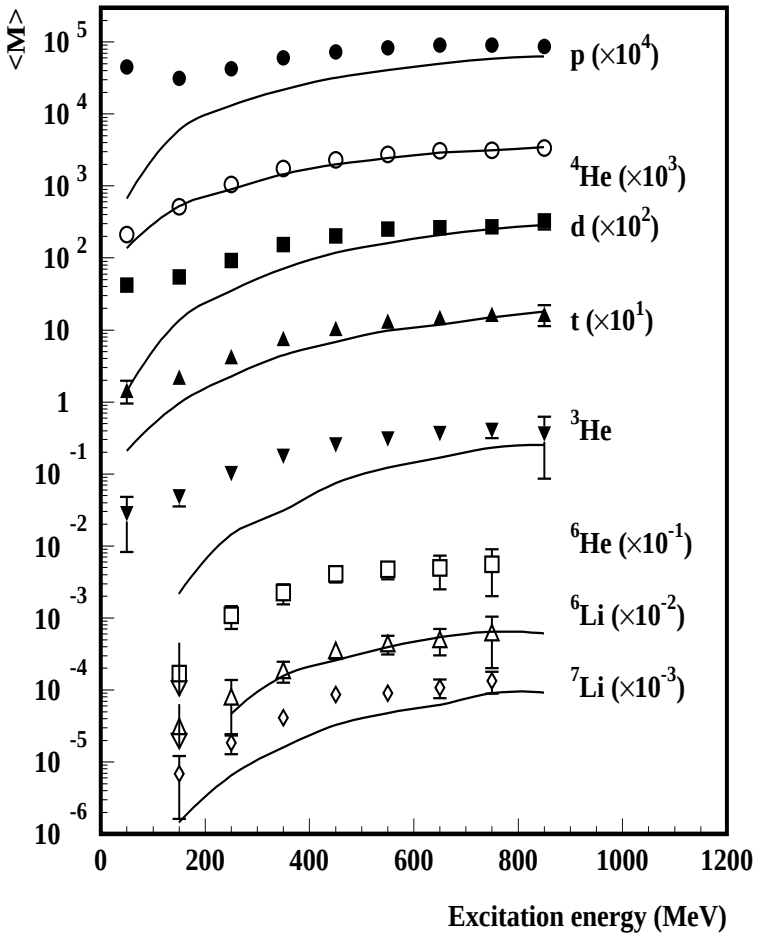

Fig. 13. Angular integrated charged-particle multiplicities as a function of excitation energy: Symbols: As determined from the measured multiplicity data (with statistical error bars included within the symbols when not apparent) not corrected for detection efficiency. Lines: As obtained from the evaporation stage of the simulation and corrected for detection acceptance (not implemented for ^{6}He). Note that table 3 also provides detailed figures (in term of multiplicities and relative abundances) related to these data.

energy among the possible decay channels. The difficulty experienced by the hybrid model to account for the measured charged-particle spectra is unlikely to be due to charged-particle auto-correlation artifacts induced by the use of the correlation E*(M$_n$, M$_{lcp}$). Charged particles do simply not carry enough excitation energy, while the neutron evaporation is the dominant decay channel of the hot and heavy target remnant. Furthermore, since the correlation E*(M$_n$, M$_{lcp}$) does not distinguish between different charged-particle types, it cannot be responsible for a bias for or against a particular species.

In contrast with the evaporative component of the proton spectra, the more direct and higher-energy (40<E<150 MeV) component of the spectra (Fig.14) is not satisfactorily reproduced by the model, especially at backward angles. In the model, these relatively low energy particles (low energy as compared to the projectile energy) are essentially released near the end of the intra-nuclear cascades. Backscattering is very unlikely to occur at the early stages of the INC, which is strongly forward peaked in the laboratory. Since nucleonic correlations and realistic Fermi motion of the nucleons are not considered in the INC model, its failure to account for high energy particle emission at backward angles can be expected. Moreover, towards the end of the INC stage, the nucleons are still treated as though their de Broglie wave lengths were still small as compared to the inter-nucleonic distance (the basic assumption of the INC treatment). This condition is certainly not fulfilled with nucleons at several tens of MeV. Therefore one cannot expect a perfect agreement between experimental and simulated data.

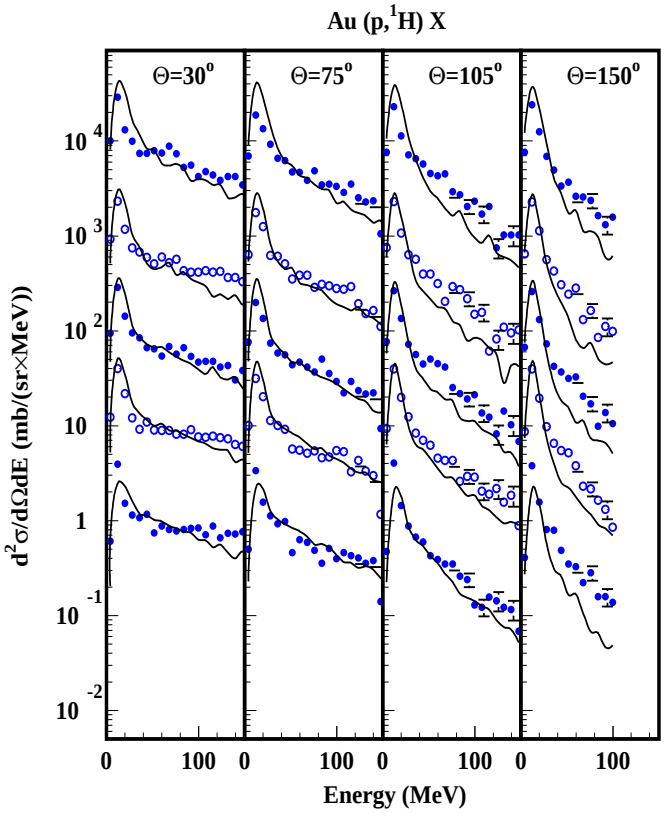

Fig. 14. Doubly differential cross sections for the proton production detected at four angles and for five E* bins (from bottom to top: E*= 0-220, 220-370, 370-470, 470-570, E* >570 MeV). The experimental data are given by dots and the simulated ones by solid lines. A 10^i factor (i = 0,...,4) has been applied from bottom to top, to the ordinate scale. The fluctuations in the curves have statistical origins.

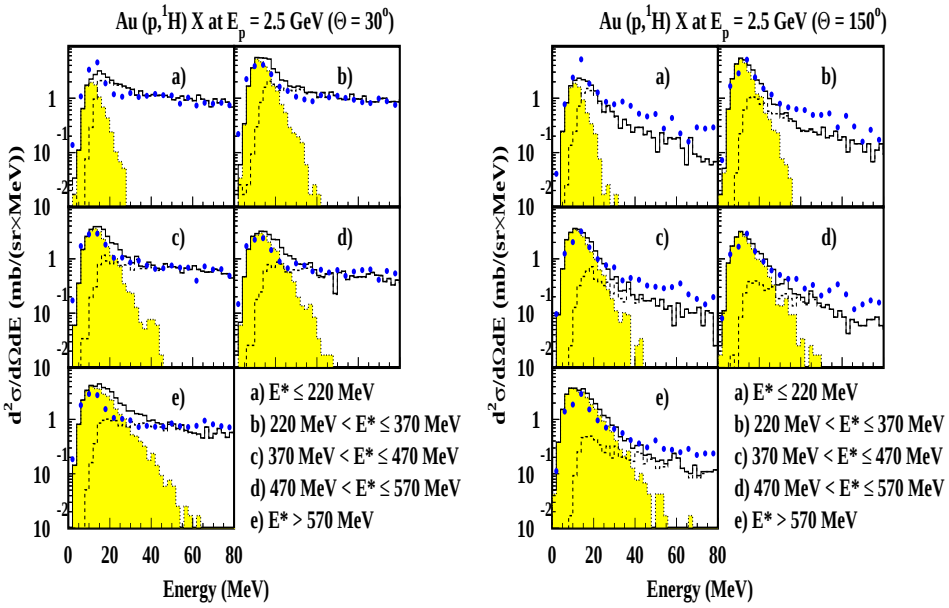

Fig. 15. Doubly differential cross sections for the proton production as obtained from experimental data (dots) at 30° and 150° for five E* bins. The shaded spectra represent the simulated evaporative contribution, the dashed histograms the simulated direct INC contribution and the solid histograms their sum.

In order to investigate the possible formation of composite-particles by coalescence during the INC stage, some modifications have been made in the INC treatment following the prescriptions by Nagle et al.[59] or Mattiello et al.[60]. Each time a nucleon is about to leave the nucleus (i.e. with an exit time shorter than the average collision time), an inspection is made over all other nucleons in order to check whether there are one or several nucleons close enough in phase space to allow the formation of a stable composite-particle (unstable di-neutrons and di-protons (^{2}He) are excluded). When matching the phase space criterium, the binding energy of the composite-particle is taken into account in the energy balance of the system. Then, as any individual nucleon, the composite-particle is either reflected on the wall of the potential well describing the nucleus or is emitted, depending on its kinetic energy. When emitted, its kinetic energy is reduced by the potential energy of its composing nucleons. When the composite-particle is reflected on the potentiel wall, its composing nucleons are set free and, all, backscattered by the wall and they become available again in the nucleus and in the INC process. This somewhat arbitrary prescription for the dynamics of composite-particle emission may lead to some underestimation of proton emission at intermediate energies, discussed further below.

In this coalescence model, composite-particles are thus not allowed being

formed in the interior of the nucleus and only the surface layer contributes effectively to their semission. This assumption appears reasonable for weakly bound quasi-deuterons but may be debatable for strongly bound particles as ^{4}He.

In the algorithm applied in the calculations, composite-particles with A>2 are formed by successive coalescence, even if the process is essentially prompt. In other words, the phase space conditions must be satisfied first for ^{2}H, before heavier particles can be formed.

For any nucleon, i, about to leave the nucleus, one considers all other nucleons, j, to compute both $r_{ij}= \mid \overrightarrow{r_i} - \overrightarrow{r_j} \mid$ and the relative momentum $p_{ij} = \frac{1}{2} \mid \overrightarrow{p_i} - \overrightarrow{p_j} \mid$. Instead of imposing the twofold condition: $p_{ij} \leq \Delta p_0$ and $r_{ij} \leq \Delta r_0$, as done for instance in [61], which would somewhat restrict the available phase space for ^{2}H formation, relative momenta and positions of coalescing nucleons are required to fulfill the condition that

$$r_{ij}.p_{ij} \leq \Delta r_0.\Delta p_0$$

The condition $r_{ij} > 1$ fm in order to take into consideration the repulsive character of the nucleon-nucleon potential at short distances is fulfilled by the INC model.

The procedure is generalized to any intermediate composite-particle, just by replacing in the preceding equations, the r_i and p_i vectors by the corresponding r_N and p_N vectors: the coordinate and momentum of the composite-particle N , respectively.

One thus gets by generalization of the preceding equation:

$$R_{N_j}= \mid \overrightarrow{R_N} - \overrightarrow{r_j} \mid \text{ and } p_{N_j}=\mid \frac{m_j}{M_N+m_j} \overrightarrow{p_N} - \frac{M_N}{M_N+m_j} \overrightarrow{p_j} \mid$$

with M_N and m_j, the masses of the intermediate composite N and nucleon j, respectively.

As a general condition for the accumulation of a further nucleon by a cluster of N nucleons one formulates:

$$R_{Nj}.P_{Nj} \leq \Delta r_0(N,j).\Delta p_0(N,j) \text{ with } R_{Nj} > 1 \text{ fm}$$

The product $\Delta r_0(N,j).\Delta p_0(N,j)$ has been adjusted for each type of composite-particle in order to reproduce its production as given by the experimental data (Table 4). Values of 336 fm.MeV/c have been deduced for the production of ^{2}H, 315 fm.MeV/c for ^{3}H (^{2}H+n) and ^{3}He (^{2}H+p) and 300 fm.MeV/c for ^{4}He (either through (^{3}H+p) or (^{3}He+n)) (Table 3). For the deuterons with 50 MeV

$<E_d<$200 MeV generated by our model, the $R_{Nj}.P_{Nj} \leq \Delta r_0(N,j).\Delta p_0(N,j)$ condition leads to $< r_{ij} >$=2.0 fm. It can also be noted that in so far as the deuteron production is concerned, one can find in Nagle et al.[59] $\Delta r_0 = 2.1$ fm and $\Delta p_0 = 150$ MeV/c leading to ($\Delta r_0.\Delta p_0 = 315$ fm MeV/c) in close agreement with the value of 336 fm.MeV/c used in the present study. It must also be stressed that in the present model these parameters have some connection between each other. Indeed, when considering the formation of either ^{3}H or ^{3}He from ^{2}H, one depletes the production of the latter composite-particle in order to produce the former. In other words, if we had ignored the production of particles with mass A>2, we would have needed $\Delta r_0.\Delta p_0$ smaller than 336 fm.MeV/c in order to fit the deuterium data.

Reaction	$\Delta r_0 \times \Delta p_0$ (fm.MeV/c)
p+n→d	336
d+n→t, d+p→^{3}He	315
t+p→^{4}He, ^{3}He+n→^{4}He	300

Table 4
Phase space parameters used in the coalescence model for the production of different composite particles.

In Fig. 16 the results of the simulations following the implementation of coalescence in the INCL2.0 code are shown at 30° for H and He isotopes together with the experimental data. The satisfactory agreement obtained for ^{2}H, ^{3}H, ^{3}He when using the above mentioned parameters for $\Delta r_0.\Delta p_0$ is not surprising since it results from a fitting procedure. However, it was impossible to fit the ^{4}He spectrum with a physically *reasonable* $\Delta r_0.\Delta p_0$ value. The simulation done for ^{4}He exhibits in Fig 16 a strong underestimation. This may arise from two types of deficiencies in the model. First, as being stressed in the description of the model, mostly nucleons at the surface of the nucleus are implied in the build-up of composite-particles. If such an assumption is reasonable for weakly bound isotopes, it might be a too severe constraint for a strongly bound α -particle. Second, the formation of an α-particle by means of two preformed clusters, ^{2}H+^{2}H, has not been implemented in the very simple model presented here.

It can be noted in Fig. 16 that the ^{1}H experimental data which were rather satisfactorily accounted for in absence of coalescence (dashed curve) are underestimated by about a factor two between 40 and 200 MeV after introduction of coalescence. The build-up of composite-particles is obviously responsible for the observed loss of ^{1}H. The conclusion for this feature can be stated as follows. Whether coalescence is implemented or not in the INC model, there is clearly in either version of the model a lack of intermediate energy (40-200 MeV) H production, either as free protons when coalescence is implemented

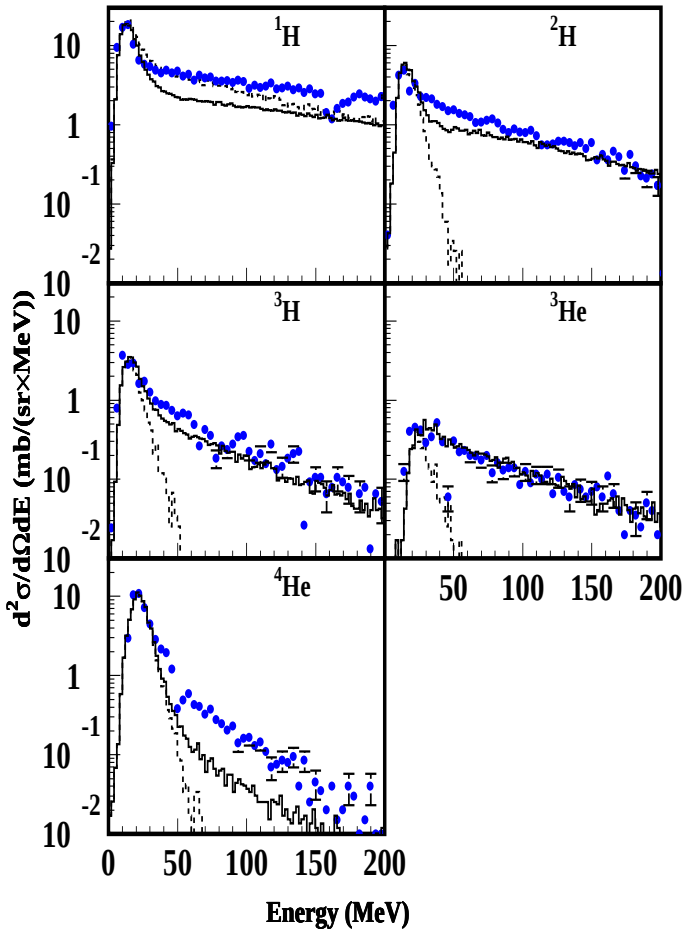

Fig. 16. Doubly differential production cross sections for the H and He isotopes as measured at 30° (dots) and as simulated in absence of coalescence in INCL2.0 (dashed histograms) and after implementation of coalescence in INCL2.0 (solid histograms).

or as composite-particles when coalescence is absent.

Fig 17-20 provide with some details (angular and E* dependences) the comparison between experimental particle production and simulated data after coalescence has been implemented in the INC step of the two-step model. The deficit of free protons with E= 40-150 MeV in the model (Fig.17) is a general feature which shows up at all angles and for all E* of the nuclei they are ejected from. In the same way, the quality of the simulated data for all composite-particles is not shown to depend sensitively on the particular emission angle or E* bin at which they are considered. This observation tells us that there are for instance no compensation effect linked to impact parameter since there is a relationship between E* and impact parameter. The quality of

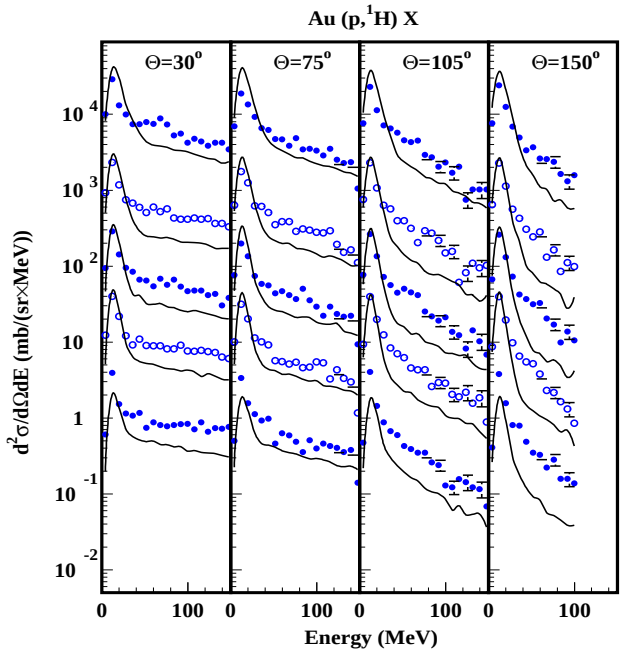

Fig. 17. Same as Fig.14 for the experimental data (dots). The solid lines are the results of the Monte-Carlo simulations taking coalescence into account (see text).

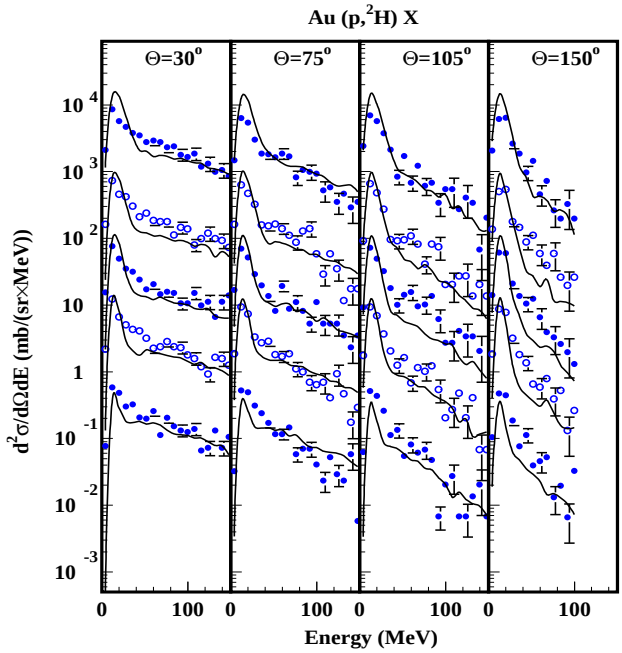

Fig. 18. same as Fig.17 for ^{2}H.

the agreement is found to be very satisfactory for ^{2}H, ^{3}H and ^{3}He emission in the detailed presentation in Figs.18-20. In some sense it is remarkable that a

rather crude model can reproduce the measured data in such detailed considerations. With the phase space parameters for coalescence being adjusted in order to fit the 30° data, there is *a priori* no obvious reason why they would allow a good reproduction of the data at other emission angles and at all E* (i.e. for all impact parameters). These good results give credit to coalescence as a process to produce these non-evaporative composite-particles. Fig. 21 exhibits the measured energy spectra for ^{4}He as a function of emission angle and excitation energy together with the corresponding calculated evaporated components (solid lines). The agreement is excellent at low energy and the non-evaporative component is shown to be very weak in all cases. However and as already shown in Fig. 16, although weak, this component is underpredicted by the present coalescence model (the modeled data are not shown in Fig.21 for sake of clarity).

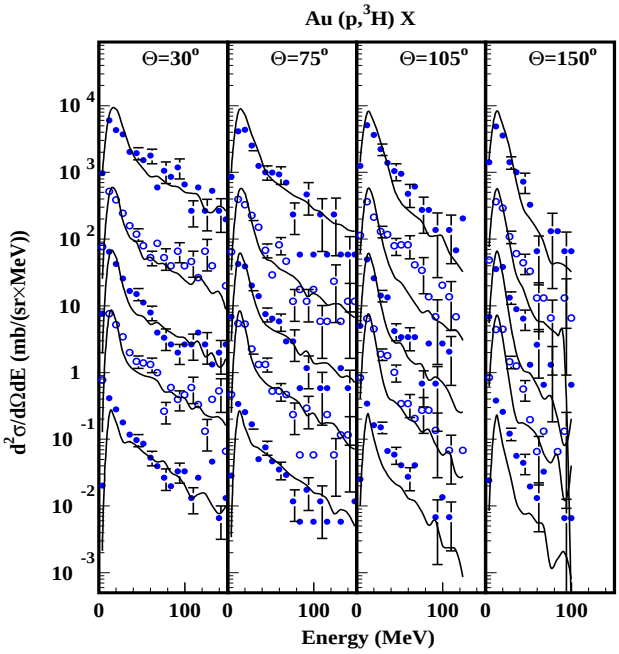

Fig. 19. same as Fig.17 for ^{3}H.

The underestimate of the emission of protons with intermediate energy in the INC/coalescence model (Fig.17) could be taken to imply that the model NN scattering cross sections are too large and, hence, proton collisions steepening the energy spectrum too frequent. More likely reasons for the observed discrepancies are the intrinsic deficiencies of the INC model, which is based on the impulse approximation and neglects nucleonic correlations leading to high and anisotropic components in the nucleonic momentum distribution. It is not clear what particular effects to expect from the violation of other prerequisites for the INC model, such as a small de Broglie wave length.

Before summarizing, some comments ought to be made about "isotopic tem-

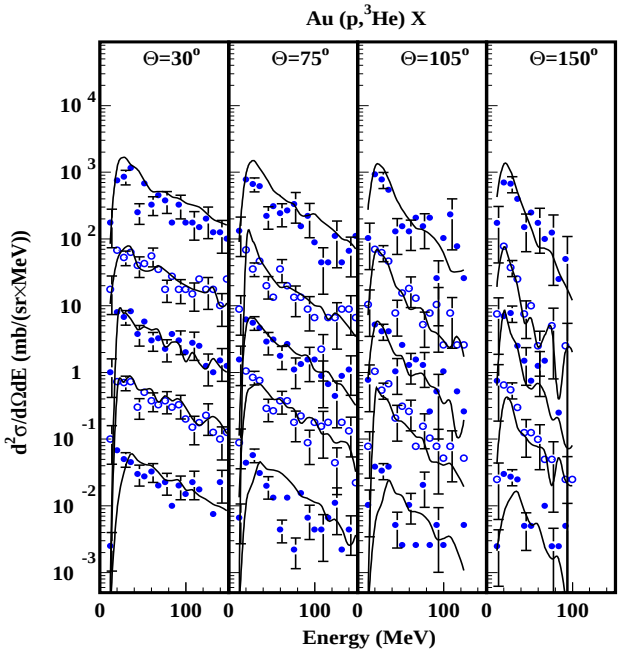

Fig. 20. same as Fig.17 for ^{3}He.

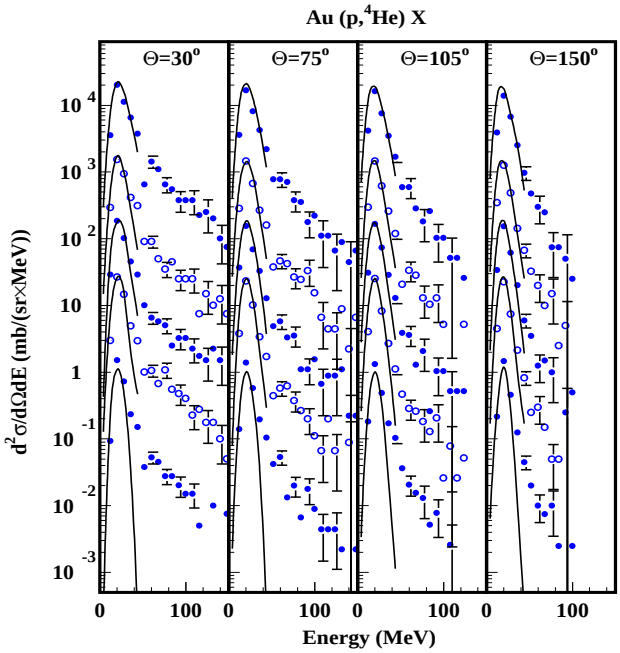

Fig. 21. same as Fig.17 for ^{4}He (the evaporative component, only, is presented by the solid line).

perature" determination in spallation reactions. In a recent publication, Andronenko et al.[62] have determined isotopic temperatures in 1 GeV proton induced reactions on a large variety of target materials by considering the

double ratios of the yields of two isotope pairs differing by one neutron each, as proposed earlier by S. Albergo et al [63]. Andronenko et al. have noticed for a given " thermometer ", i.e. a given set of pairs of considered particles, a constancy of the deduced temperature for a wide range of bombarded targets (from Be up to U). In the light of the present 2.5 GeV p+Au data, we can make several comments relative to the determination of isotopic temperatures in Ref.[62].

- Firstly, as shown in Fig.8 of the present paper, by selecting exit channels implying the emission of a low-energy charged particle one disregards the low E* events, those for which only neutrons are evaporated. These events are particularly abundant for heavy targets and at low E* due to the large Coulomb barrier effects. As a consequence of this charged particle selection, the deduced isotopic temperature is artificially increased as compared to what would be a weighted temperature including *all* decay channels and this is all the more important as the atomic number of the bombarded target is increased. Thus, the isotopic thermometer approach introduces a bias on T which is moreover target size dependent.

- Secondly, to make sense, only particles issued from a fully thermalized system should be considered in order to infer a temperature. The data of Table 2 show that this condition is difficult to fulfill and that there are large differences in the behavior of neighboring isotopes, e.g. ^{4}He is mostly of evaporative origin while ^{3}He is dominated by direct non-equilibrium emission. If this situation is less critical at backward angles, Fig.5 shows that, for some products (like ^{1}H, ^{3}He), evaporation is never dominant even when considering emission in the most backward direction. Moreover and as shown in Table 3, the contamination of evaporative by non-evaporative emission depends strongly on the excitation energy reached by the impinged nucleus, with the strongest contamination at relatively low E* and thus also for the most abundant events. Although it could not be shown in the present work with a single target nucleus explored, there is no doubt that the relative amount of non-evaporated particles with respect to that of evaporated ones depends strongly on the size of the target nucleus. This must introduce an additional bias in the comparison of the isotopic temperatures thus inferred for different target sizes.

Considering all the above comments, we have not attempted to use the relative population of isotopes to infer "isotopic temperatures" in the present paper. Neither did we try determining "spectral temperatures" from the slopes of the measured energy spectra because of the contamination by non-equilibrium particles. Even ^{4}He, the particle with the *purest* evaporative character, cannot be used for this purpose because the non-evaporative component is located mostly in the tail of the energy spectrum, thus strongly modifying the slope of this tail.

4 SUMMARY

Neutron-, proton-, and light composite-particle (H, He and Li isotopes) emissions have been investigated in detail in the 2.5 GeV proton p + Au reaction, using two high-efficiency neutron and charged particle detectors coupled with high resolution telescopes. The present study has been focused on the emission of composite-particles which are only partially accounted for by a standard two-step spallation model. Indeed, in the latter, composite-particle emission is considered in the evaporation stage but not in the initial intra nuclear cascade stage.

The comparison of model simulations with experimental data gives some confidence in a realistic representation of the p+Au reaction scenario by the INC/GEMINI hybrid model. For example, the model predicts correctly the excitation energy of the target at the end of the INC. This conclusion is based on a comparison of theoretical and experimental multiplicity correlations suggesting an average calibration of the excitation energy, $E^*=E^*(M_n, M_{lcp})$. The accuracy of this approach is shown to depend on the explored domain of E^*. This effect is attributed to varying contributions by non-statistical particles which are indistinguishable from the evaporated particles and upset the relation between multiplicity and energy carried away per particle. This is also due to the finite detection efficiency of the detectors: even when using highly efficient ones ($\varepsilon \approx 80\%$ for *both* the BSiB *and* the BNB) as in the present experiment, one should be cautious to take the efficiency into account.

The main deviation between the model *in its standard version* and experimental data concerns the composite-particles in their high energy part. The model reproduces quite successfully the low-energy, evaporative part of their spectra, but misses the high-energy tails. Coalescence has been assumed to be a likely mechanism for the emission of high-energy composite-particles. A prescription for the recognition of composite-particles has been implemented in the standard INC model, based on the proximity of nucleon in phase space. A coalescence domain has been defined in terms of somewhat arbitrary parameters. As expected, this coalescence mechanism depletes the high-energy proton channel, in particular for proton energies between 40 and 150 MeV and leads to a corresponding discrepancy with the data. Most likely, this deficit points at a general difficulty inherent in INC when this model is run all the way until thermal equilibrium is achieved. In the last steps of the stage towards equilibrium, the basic requirement of the model concerning the upper values of the de Broglie wave lengths of the cascade particles is no longer met. Such a weakness of the model has long been recognized but so far it was generally ignored since the gross observables deduced from the model were found in satisfactory agreement with available data. These problems were also partially hidden because the overall weight of these, non-evaporative, composite-particles remains gen-

erally weak as compared to those of equilibrium origin. It is the advantage of more and more exclusive and precise measurements to reveal the shortcomings of the current model.

How the deficiencies in the current model can be cured is a difficult question to answer. The introduction of an intermediate pre-equilibrium model between INC and the evaporation process, often considered as an improvement, simply shifts the difficulties but does not remove them. Indeed, the link between INC and pre-equilibrium is also very difficult to make, with some nucleons being still above the threshold of applicability of INC (say E>200 MeV) while others are already below

In absence of a more sophisticated description of the whole process, INCL2.0 with its 2 options (coalescence implemented or not) can thus still be very useful for a satisfactory simulation of the production of particles (neutrons, protons without implementing coalescence and composite-particles when implementing coalescence). As was also shown by Enke et al.[3], INCL2.0 does a much better job for heavy target-nuclei than the most commonly used High Energy Transport Codes (e.g. LAHET or HERMES) as far as the E*-distribution is concerned.

Finally, one should mention the recent development of a quantum molecular dynamics (QMD) approach in proton induced reactions as a first step replacing the more conventional INC treatment[64]. This approach predicts the dynamical formation of light fragments but so far -to our knowledge and understanding- such a calculation has been restricted to rather light targets (Al and Fe) because of excessive computation time on massive targets.

Acknowledgments

We are indebted to the COSY staff for the good beam quality. We thank J.Cugnon for providing us with the INCL2.0 version of his computer code and for enlightening discussions. This work was supported by the EU TMR-project ERB-FMRX-CT98-0244, by the french GEDEON project and the German Strategiefonds project R&D for ESS of the Helmholtz Gesellschaft.

References

[1] L.Pienkowski, H.G.Bohlen, J.Cugnon, H.Fuchs, J.Galin, B.Gatty, B.Gebauer, D.Guerreau, D.Hilscher, D.Jacquet, U.Jahnke, M.Josset, X.Ledoux, S.Leray, B.Lott, M.Morjean, A.Péghaire, G.Röschert, H.Rossner, R.H.Siemssen and C.Stéphan, Phys. Lett. B 336 (1994) 147.

[2] X.Ledoux, H.G.Bohlen, J.Cugnon, H.Fuchs, J.Galin, B.Gatty, B.Gebauer,

D.Guerreau, D.Hilscher, D.Jacquet, U.Jahnke, M.Josset, S.Leray, B.Lott, M.Morjean, B.M.Quednau, G.Röschert, H.Rossner, A.Péghaire, L.Pienkowski, R.H.Siemssen and C.Stéphan, Phys. Rev. C 57 (1998) 2375.

[3] M.Enke, C.M.Herbach, D.Hilscher, U.Jahnke, O.Schapiro, A.Letourneau, J..Galin, F.Goldenbaum, B.Lott, A.Péghaire, D.Filges, R.D.Neef, K.Nünighoff, N.Paul, H.Schaal, G.Sterzenbach, A.Tietze and L.Pienkowski, Nucl. Phys. A 657 (1999) 317

[4] C.M.Herbach, M.Enke, D.Hilscher, U.Jahnke, V.Tishchenko, A.Letourneau, A.Böhm, J.Galin, B.Lott, A.Péghaire, D.Filges, F.Goldenbaum, R.D.Neef, K.Nünighoff, N.Paul, H.Schaal, G.Sterzenbach, L.Pienkowski, W.U.Shröder, J.Tõke, Proceedings of SARE-5 Meeting, July 17-21, 2000, OECD Paris.

[5] R.Michel, M.Gloris, H.J.Lange, I.Leya, M.Lüpke, U.Herpers, B.Dittrich-Hannen, R.Rösel, Th.Schiekel, D.Filges, P.Dragovitsch, M.Suter, H-J.Hofmann, W.Wölfli, P.W.Kubik, H.Baur and R.Wieler, Nucl. Inst. Meth. B 103 (1995) 183.

[6] L.Pienkowski, F.Goldenbaum, D.Hilscher, U.Jahnke, J.Galin and B.Lott, Phys. Rev. C 56 (1997) 1909.

[7] D.Hilscher, U.Jahnke, F.Goldenbaum, L.Pienkowski, J.Galin and B.Lott, Nucl. Instr. and Meth. A 414 (1998) 100.

[8] B.Lott, F.Cnigniet, J.Galin, F.Goldenbaum, D.Hilscher, A.Liénard, A.Péghaire, Y.Périer and X.Qian, Nucl. Instr. and Meth. A 414 (1998) 117.

[9] S.Meigo, H.Takada, S.Chiba, T.Nakamoto, K.Ishibashi, N.Matsufuji, K.Maehata, N.Shigyo, Y.Watanabe and M.Numajiri, Nucl. Inst. Meth. A 431 (1999) 521.

[10] X.Ledoux, F.Borne, A.Boudard, F.Brochard, S.Crespin, D.Drake, J.C.Duchazeaubeneix,D.Durand, J.M.Durand, J.Fréhaut, F.Hanappe, L.Kowalski, C.Lebrun, F.R.Lecolley, J.F.Lecolley, F.Lefebvres, R.Legrain, S.Leray, M.Louvel, E.Martinez, S.I.Meigo, S.Ménard, G.Milleret, Y.Patin, E.Petibon, F.Plouin, P.Pras, L.Stugge, Y.Terrien, J.Thun, M.Uematsu, C.Varignon, D.M.Whittal and W.Wlazlo, Phys. Rev. Lett. 82 (1999) 4412.

[11] F.Rejmund, B.Mustapha, P.Armbruster, J.Benlliure, M.Bernas, A.Boudard, J.P.Dufour, T.Enqvist, R.Legrain, S.Leray, K-H.Schmidt, C.Stéphan, J.Taieb, L.Tassan-got and C.Volant,Nucl. Phys. A 683 (2001) 540.

[12] T.Enqvist, W.Wlazło, P.Armbruster, J.Benlliure, M.Bernas, A.Boudard, S.Czajkowski, R.Legrain, S.Leray, B.Mustapha, M.Pravikoff, F.Rejmund, K.H.Schmidt, C.Stéphan, J.Taieb, L.Tassan-Got and C.Volant, Nucl. Phys. A 686 (2001) 481.

[13] J.Benlliure, P.Armbruster, M.Bernas, A.Boudard, J.P.Dufour, T.Enqvist, R.Legrain, S.Leray, B.Mustapha, F.Rejmund, K.H.Scmidt, C.Stéphan, L.Tassan-Got and C.Volant, Nucl. Phys. A 683 (2001) 513.

[14] W.Wlazło, T.Enqvist, P.Armbruster, J.Benlliure, M.Bernas, A.Boudard, S.Czajkowski, R.Legrain, S.Leray, B.Mustapha, M.Pravikoff, F.Rejmund, K.H.Schmidt, C.Stéphan, J.Taieb, L.Tassan-got and C.Volant, Phys. Rev. Lett. 84 (2000) 5736.

[15] E.C.Pollacco, J.Brzychczyk, C.Volant, R.Legrain, R.G.Korteling, D.S.Bracken, K.Kwiatkowski, K.B.Morley, E.Renshaw Foxford, V.E.Viola, N.R.Yoder, H.Breuer and J.Cugnon, Phys. Lett. B 482 (2000) 349.

[16] F.Goldenbaum, W.Bohne, J.Eades, T.v.Egidy, P.Figuera, H.Fuchs, J.Galin, Ye.S.Golubeva, K.Gulda, D.Hilscher, A.S.Iljinov, U.Jahnke, J.Jastrzebski, W.Kurcewicz, B.Lott, M.Morjean, G.Pausch, A.Péghaire, L.Pienkowski, D.Polster, S.Proschitzki, B.Quednau, H.Rossner, S.Schmid, W.Schmid and P.Ziem, Phys. Rev. Lett. 77 (1996) 1230.

[17] L.Pienkowski, W.Bohne, T.von Egidy, P.Figuera, J.Galin, F.Goldenbaum, D.Hilscher, U.Jahnke, J.Jastrzebski, B.Lott, M.Morjean, G.Pausch, A.Péghaire, D.Polster, S.Proschitzki, B.Quednau, H.Rossner, S.Schmid and W.Schmid, Phys. Lett. B 472 (2000) 15.

[18] B.Lott, F.Goldenbaum, A.Böhm, W.Bohne, T.von Egidy, P.Figuera, J.Galin, D.Hilscher, U.Jahnke, J.Jastrzebski, M.Morjean, G.Pausch, A.Péghaire, L.Pienkowski, D.Polster, S.Proschitzki, B.Quednau, H.Rossner, S.Schmid and W.Schmid, Phys. Rev. C 63 (2001) 034616.

[19] T.von Egidy, P.Figuera, J.Galin, F.Goldenbaum, Ye.S.Golubeva, M.Hasinoff, D.Hilscher, A.S.Iljinov, U.Jahnke, M.Krause, W.Kurcewicz, X.Ledoux, B.Lott, L.Maier, M.Manrique de Lara, G.Pausch, L.Pienkowski, B.Quednau, W.Schott, W.U.Schröder and J.Tőke, Eur. Phys. Journal A , 8 (2000) 197.

[20] U.Jahnke, W.Bohne, T.von Egidy, P.Figuera, J.Galin, F.Goldenbaum, D.Hilscher, J.Jastrzebski, B.Lott, M.Morjean, G.Pausch, A.Péghaire, L.Pienkowski, D.Polster, S.Proschitzki, B.Quednau, H.Rossner, S.Schmid and W.Schmid, Phys. Rev. Lett. 83 (1999) 4959.

[21] T.Lefort, K.Kwiatkowski, W.-c. Hsi, L.Pienkowski, L.Beaulieu, B.Back, H.Breuer, S.Gushue, R.G.Korteling, R.Laforest, E.Martin, E.Ramakrishnan, L.P. Remsberg, D.Rowland, A.Ruangma, V.E.Viola, E.Winchester and S.J.Yennello, Phys. Rev. Lett. 83 (1999) 4033.

[22] P.J.Bryant, Nucl. Phys. B 51A (1996) 125.

[23] J.M.Carpenter, T.A.Gabriel, E.B.Iverson and D.W.Jerng, Physica B 270 (1999) 272.

[24] ISIS facility, Annual Report 1998-1999.

[25] PSI Scientific and Technical Report 2000, Vol. VI, ISSN 1423-7350, March 2001.

[26] The European Spallation Source Study, vol. III, The ESS Technical Study, report ESS-96-53-M, 1996, ISBN 0902376659.

[27] H.Arnould et al., Phys. Lett. B 458 (1999) 167.

[28] A.Abánades et al., Nucl. Inst. Meth. A 463 (12001) 586.

[29] J.-S. Wan et al., Nucl. Inst. Meth. A 463 (12001) 634.

[30] C.D.Bowman, E.D.Arthur, P.W.Lisowski, G.P.Lawrence, R.J.Jensen, J.L.Anderson, B.Blind, M.Cappiello, J.W.Davidson, T.R.England, L.N.Engel, R.C.Haight, H.G.Hughes III, J.R.Ireland, R.A.Krakowski, R.J.LaBauve, B.C.Letellier, R.T.Perry, G.J.Russel, K.P.Staudhammer, G.Versamis and W.B.Wilson, Nucl. Instr. Meth. Phys. Res. A 320 (1992) 336.

[31] C.Rubbia, J.A.Rubio, S.Buono, F.Carminati, N.Fiétier, J.Galvez, C.Gelès, Y.Kadi, R.Klapisch, P.Mandrillon, J.P.Revol and C.H.Roche, Report No. CERN/AT/95-44(ET) (1995).

[32] A.Letourneau, J.Galin, F.Goldenbaum, B.Lott, A.Péghaire, M.Enke, D.Hilscher, U.Jahnke, K.Nünighoff, D.Filges, R.D.Neef, N.Paul, H.Schaal, G.Sterzenbach and A.Tietze, Nucl. Inst. Meth. B 170 (2000), 299.

[33] M.A.Lone and P.Y.Wong, Nucl. Inst. Meth. A 362 (1995) 499.

[34] Yu.E.Titarenko, O.V.Shvedov, M.M.Igumnov, S.G.Mashnik, E.I.Karpikhin, V.D.Kazaritsky, V.F.Batyaev, A.B.Koldobsky, V.M.Zhivun, A.N.Sosnin, R.E.Prael, M.B.Chadwick, T.A.Gabriel and M.Blann, Nucl. Inst. Meth. A 414 (1998) 73.

[35] L.A.Charlton, E.Jerde, D.C.Glasgow and T.A.Gabriel, Nucl. Inst. Meth. A 425 (1999) 371.

[36] S.G.Mashnik, A.J.Sierk, O.Bersillon and T.Gabriel, Nucl. Inst. Meth. A 414 (1998) 68.

[37] J.Cugnon, Nucl. Phys. A 462 (1987) 751.

[38] A.M.Poskanzer, G.W.Butler, E.K.Hyde, Phys. Rev. C 3 (1971) 882.

[39] E.K.Hyde, G.W.Butler, A.M.Poskanzer, Phys. Rev. C 4 (1971) 1759.

[40] G.D.Westfall, R.G.Sextro, A.M.Poskanzer, A.M.Zebelman, G.W.Butler, E.K.Hyde, Phys. Rev. C 17 (1978) 1368.

[41] R.E.L.Green and R.G.Korteling, Phys. Rev. C 22 (1980) 1594.

[42] R.E.L.Green, R.G.Korteling, J.M.D'Auria, K.P.Jackson and R.L.Helmer, Phys. Rev. C 35 (1987) 1341.

[43] A. Fokin, L. Carlén, R. Ghetti, B.Jakobsson, J.Mårtesson, Yu.Murin, A.Oskarsson, C.Ekström, G.Ericsson, J.Romanski, E.J.vanVeldhuizen, L.Westerberg, K.Nybö, T.F.Thorteinsen, S.Amirelmi, M.Guttormsen, G.Løvhøiden, V.Bellini, F.Palazzolo, M.L.Sperduto, J.P.Bondorf, I.Mishustin, V.Avdeichikov, O.V.Lozhkin, W.A.Friedman and K.K.Gudima, Phys. Rev. C 60 (1999) 024601

[44] D.B.Barlow, B.M.K.Nefkens, C.Pillai, J.W.Price, I. Slaus, M.J.Wang, J.A.Wightman, K.W.Jones, M.J.Leitch, C.S.Mishra, C.L.Morris, J.C.Peng, P.K.Teng and J.M.Tinsley, Phys. Rev. C 45 (1992) 293.

[45] M.Büscher, A.A. Sibirtsev and K.Sistemich, Z. Phys. A 350 (1994) 161

[46] S.T.Butler and C.A.Pearson, Phys. Rev. 129 (1962) 836.

[47] P.Figuera, W.Bohne, B.Drescher, F.Goldenbaum, D.Hilscher, U.Jahnke, B.Lott, L.Pienkowski and P.Ziem, Z.Phys. A 352 (1995) 315.

[48] C.M.Herbach et al., to be published.

[49] J.Galin and U.Jahnke, Nucl. Part. Phys. 20 (1994) 1105.

[50] N.Marie and the INDRA collaboration, Phys. Lett. 391 B (1997) 15.

[51] H.W.Bertini, Phys. Rev. 131 (1963) 1801.

[52] R.E.Prael, H.Lichtenstein, LAHET code system LAHET 2.7d, Los Alamos National Laboratory Report LA-UR-89-3014 (1989)

[53] P.Cloth, D.Filges, R.D.Neef, G.Sterzenbach, Ch.Reul, T.W.Armstrong, B.L.Colborn, B.Anders, H.Brückmann, Report Jülich 2203 (1988).

[54] J.Cugnon, C.Volant and S.Vuillier, Nucl. Phys. A 620 (1997) 475.

[55] J.Cugnon, S.Leray, E.Martinez, Y.Patin and S.Vuillier, Phys. Rev. C 56 (1997) 2431.

[56] W.U.Schroeder, Nucl. Phys. A 538 (1992) 439c

[57] J.Toke, D.KAgnihotri, W Skulski and W.U.Schroeder, Phys. Rev. C 63 (2001) 024604-1

[58] R.J.Charity, M.A.McMahan, G.J.Wozniak, R.J.McDonald, L.G.Moretto, D.G.Sarantites, L.G.Sobotka, G.Guarino, A.Pantaleo, L.Fiore, A.Gobbi and K.D.Hildenbrand, Nucl. Phys. A 483 (1988) 371 (GEMINI-code obtained via ftp from wunmr.wustl.edu).

[59] J.L.Nagle, B.S. Kumar, D.Kusnezov, H.Sorge and R.Mattiello, Phys. Rev. C 53 (1996) 367.

[60] R. Mattiello, H.Sorge, H.Stöcker and W.Greiner, Phys. Rev. C 55 (1997) 1443.

[61] A.J.Baltz, C.B.Dover, S.H.Kahana, Y.Pang, T.J.Schlagel and E.Schnedermann, Phys. Lett. B 325 (1994) 7.

[62] M.N.Andronenko, L.N. Andronenko, W.Neubert and D.M.Seliverstov, Eur. Phys. J. A 8 (2000) 9.

[63] S.Albergo et al., Nuovo Cimento Soc. Ital. Fis. 89A (1985) 1

[64] S.Chiba, O.Iwamoto, T.Fukahori, K.Niita, T.Maruyama, T.Maruyama and A.Iwamoto, Phys. Rev. C 54 (1996) 285.

5 APPENDIX

Table 3
Average multiplicities of charged particles as a function of excitation energy with: $< M >_{total}$, as determined from the experimental data and including all *detected* particles. Note that the energetic particles that exceeds the upper detection thresholds (mostly emitted during the INC stage) are thus not included in these figures. $< M >_{evaporated}$, as given by the evaporation step of the simulation and folded with the detection efficiency. $< M >_{direct} = < M >_{total} - < M >_{evaporated}$ The last column provides the approximated ratio of direct to total emission when reasonable uncertainties make it meaningful. It can be noted that at low E*, direct charged particle emission is overwhelming and that the given figures depend strongly upon the location of the most forward telescope(s).

	E* (MeV)	$< M >_{total}$	$< M >_{evaporated}$	$< M >_{direct}$	$\frac{<M>_{dir}}{<M>_{tot}}$
	0-100	4.51 ± 0.29	0.067 ± 0.008	4.44 ± 0.30	99%
	100-200	3.12 ± 0.15	0.59 ± 0.02	2.53 ± 0.17	80
	200-300	4.23 ± 0.15	1.30 ± 0.03	2.93 ± 0.18	70
	300-400	6.00 ± 0.19	2.17 ± 0.05	3.83 ± 0.24	65
^{1}H	400-500	7.29 ± 0.22	3.19 ± 0.07	4.09 ± 0.29	55
	500-600	8.36 ± 0.28	4.06 ± 0.10	4.30 ± 0.38	50
	600-700	9.08 ± 0.43	4.99 ± 0.15	4.08 ± 0.58	45
	700-800	9.07 ± 0.69	5.84 ± 0.24	3.23 ± 0.93	35
	800-900	8.66 ± 1.35	6.33 ± 0.35	2.33 ± 1.70	25
	0-100	0.42 ± 0.09	0.014 ± 0.003	0.40 ± 0.09	95
	100-200	0.55 ± 0.05	0.134 ± 0.009	0.41 ± 0.06	75
	200-300	0.92 ± 0.06	0.35 ± 0.01	0.57 ± 0.07	60
	300-400	1.54 ± 0.09	0.71 ± 0.02	0.83 ± 0.11	55
^{2}H	400-500	2.04 ± 0.10	1.18 ± 0.03	0.86 ± 0.13	40
	500-600	2.54 ± 0.13	1.61 ± 0.05	0.93 ± 0.19	35
	600-700	2.65 ± 0.21	2.08 ± 0.08	0.57 ± 0.29	20
	700-800	2.72 ± 0.35	2.53 ± 0.13	0.19 ± 0.48	5
	800-900	3.28 ± 0.80	2.88 ± 0.21	0.40 ± 1.00	
	0-100	0.15 ± 0.05	0.021 ± 0.004	0.12 ± 0.06	85
	100-200	0.22 ± 0.03	0.095 ± 0.007	0.13 ± 0.04	55
	200-300	0.43 ± 0.04	0.23 ± 0.01	0.20 ± 0.05	45

	300-400	0.76 ± 0.06	0.45 ± 0.02	0.32 ± 0.08	40
^{3}H	400-500	1.05 ± 0.07	0.68 ± 0.03	0.37 ± 0.10	35
	500-600	1.34 ± 0.10	0.97 ± 0.04	0.36 ± 0.14	25
	600-700	1.50 ± 0.16	1.18 ± 0.06	0.32 ± 0.22	20
	700-800	1.66 ± 0.26	1.50 ± 0.09	0.16 ± 0.34	10
	800-900	1.66 ± 0.54	1.80 ± 0.13	0.02 ± 0.67	
	0-100	0.03 ± 0.02	0.000 ± 0.000	0.03 ± 0.02	100
	100-200	0.05 ± 0.02	0.002 ± 0.001	0.05 ± 0.02	95
	200-300	0.10 ± 0.02	0.014 ± 0.002	0.09 ± 0.02	85
	300-400	0.18 ± 0.02	0.031 ± 0.005	0.14 ± 0.02	80
^{3}He	400-500	0.25 ± 0.03	0.074 ± 0.007	0.18 ± 0.03	70
	500-600	0.31 ± 0.03	0.12 ± 0.01	0.19 ± 0.05	60
	600-700	0.37 ± 0.06	0.17 ± 0.02	0.20 ± 0.08	55
	700-800	0.41 ± 0.09	0.23 ± 0.03	0.17 ± 0.1	40
	800-900	0.36 ± 0.3	0.25 ± 0.05	0.10 ± 0.3	
	0-100	0.21 ± 0.04	0.14 ± 0.01	0.08 ± 0.05	
	100-200	0.52 ± 0.04	0.52 ± 0.02	0.00 ± 0.06	
	200-300	1.05 ± 0.05	0.89 ± 0.02	0.16 ± 0.07	15
	300-400	1.76 ± 0.07	1.46 ± 0.03	0.30 ± 0.10	15
^{4}He	400-500	2.31 ± 0.09	1.98 ± 0.05	0.32 ± 0.14	15
	500-600	2.75 ± 0.11	2.44 ± 0.07	0.32 ± 0.18	10
	600-700	3.09 ± 0.19	2.90 ± 0.09	0.19 ± 0.28	5
	700-800	3.13 ± 0.28	3.11 ± 0.14	0.02 ± 0.42	1
	800-900	3.38 ± 0.69	3.38 ± 0.20	0.00 ± 0.89	
	100-200	0.002 ± 0.003			
	200-300	0.011 ± 0.004			
	300-400	0.023 ± 0.007			
^{6}He	400-500	0.04 ± 0.01	not implemented		
	500-600	0.05 ± 0.01			
	600-700	0.05 ± 0.02			
	700-800	0.06 ± 0.03			

	100-200	0.003 ± 0.003	0.001 ± 0.001	0.002 ± 0.004	
	200-300	0.008 ± 0.006	0.005 ± 0.001	0.003 ± 0.007	
	300-400	0.019 ± 0.006	0.016 ± 0.003	0.003 ± 0.009	
^{6}Li	400-500	0.035 ± 0.008	0.026 ± 0.004	0.010 ± 0.01	
	500-600	0.04 ± 0.01	0.04 ± 0.007	0.005 ± 0.02	
	600-700	0.05 ± 0.02	0.05 ± 0.01	0.001 ± 0.03	
	700-800	0.06 ± 0.04	0.06 ± 0.01	0.001 ± 0.05	
	100-200	0.007 ± 0.005	0.001 ± 0.001	0.005 ± 0.006	
	200-300	0.019 ± 0.006	0.006 ± 0.002	0.012 ± 0.008	
	300-400	0.041 ± 0.009	0.016 ± 0.003	0.025 ± 0.01	
^{7}Li	400-500	0.09 ± 0.01	0.032 ± 0.005	0.05 ± 0.02	
	500-600	0.09 ± 0.02	0.048 ± 0.008	0.04 ± 0.03	
	600-700	0.11 ± 0.03	0.06 ± 0.01	0.05 ± 0.04	
	700-800	0.14 ± 0.05	0.09 ± 0.02	0.04 ± 0.07	